Cleaner Energy Systems 8 (2024) 100113

Contents lists available at ScienceDirect

Cleaner Energy Systems

journal homepage: www.elsevier.com/locate/cles

Design, modeling, and optimization of a novel 6 kWe hybrid solid oxide fuel cell high temperature-proton exchange membrane fuel cell system

Alexandros Arsalis *

FOSS Research Centre for Sustainable Energy, University of Cyprus, Kallipoleos 75, Nicosia 1678, Cyprus

ARTICLE INFO

Keywords:
Solid oxide fuel cell
Proton exchange membrane fuel cell
Fuel cell-fuel cell system
Hybrid system
Polybenzimidazole
Optimization

ABSTRACT

This work investigates a novel approach in terms of design, configuration, heat integration and optimization of a 6 kWe total energy system fueled with natural gas. Specifically, a Solid Oxide Fuel Cell (SOFC) is used for both electricity generation and fuel reforming, since its exhaust stream fuels a polybenzimidazole (PBI)-based, High Temperature-Proton Exchange Membrane Fuel Cell (HT-PEMFC). The study investigates the possible advantages of such a system in both technical and economic terms. After modeling each component/subsystem, the total system model is optimized with the objective function aiming to maximize the net electrical efficiency of the total hybrid system. The system is optimized with a genetic algorithm-based optimization strategy, reaching a net electrical efficiency of 43.6 %. In comparison to standalone fuel cell systems with the same net electrical power output, the proposed hybrid system outperforms both an HT-PEMFC system and an SOFC system, which perform at net electrical efficiencies of 23.2 % and 40.7 %, respectively. Also, the lifecycle cost for the proposed system is $64,097, which is lower than both standalone HT-PEMFC and SOFC systems. Therefore, with the current high rising costs for natural gas, such highly efficient systems are likely to become important elements of the future energy infrastructure.

Introduction

The generation of electricity in a hydrocarbon-fueled energy system is always desired to be generated at the highest possible net electrical efficiency, since this translates to significant advantages, namely lower fuel consumption and decreased carbon emissions (Rangel-Hernández et al., 2020). Fuel cell technology is very promising in these regards, since it is an electrochemical method, where hydrogen is directly converted to electricity without the high energy losses encountered in conventional heat engines (Arsalis, 2019). The most promising fuel cell technologies are Solid Oxide Fuel Cells (SOFCs) and Proton Exchange Membrane Fuel Cells (PEMFCs) (Barbir, 2013). While both of these technologies can reach very high net electrical efficiencies, when fueled directly with hydrogen, in more cost-effective conditions, hydrogen is produced from hydrocarbons, commonly natural gas (Arsalis, 2008; Arsalis et al., 2011). A practical natural gas-fueled SOFC system requires an external reforming step (pre-reformer) in addition to the internal reforming process, which occurs within the SOFC due to its high operating temperature (Calise et al., 2006b). On the other hand, a natural gas-fueled PEMFC-based system requires even more demanding fuel processing. Specifically, in addition to the conversion of natural gas to a hydrogen-rich mixture (commonly referred as synthesis gas or *syngas*), it also requires significant reduction of the CO content (Kim et al., 2011). Such shift rectors are needed to reduce the CO content to a level acceptable for fueling the PEMFC stack, without reduction of its performance through fast degradation of the membrane (O'Hayre et al., 2009). High temperature-PEMFC (HT-PEMFC) technology is based on the polybenzimidazole (PBI) material, which allows operation at higher temperatures, in comparison to more conventional Nafion-based PEMFC technology (specifically 140–180 °C instead of 60–90 °C) (Arsalis et al., 2011). HT-PEMFC-based systems are therefore more advantageous when they are fueled with syngas, since they are more tolerant to relatively high CO contents (Stolten, 2010). This allows simplification of the syngas cleaning process, with the inclusion of a single Water Gas Shift (WGS) reactor, instead of several reactors, e.g., high, and low temperature WGS, and Preferential Oxidation reactors, as in the case of Nafion-based PEMFCs (Siegel et al., 2011).

Since 2000, several attempts have been made to design and model hybrid fuel cell-fuel cell systems. These attempts have been almost entirely limited to the combination of Nafion-based PEMFCs with SOFCs, where the heat generated from the SOFC subsystem is recovered

* Corresponding author.
E-mail address: arsalis@ucy.ac.cy.

https://doi.org/10.1016/j.cles.2024.100113
Received 30 January 2023; Received in revised form 24 February 2024; Accepted 24 February 2024
Available online 29 February 2024
2772-7831/© 2024 The Author(s). Published by Elsevier Ltd. This is an open access article under the CC BY license (http://creativecommons.org/licenses/by/4.0/).

Nomenclature

A_s	Fuel cell active area [m^2]
c_o	Molar concentration [kmol/m^3]
C_i	Conductivity constant [1/(Ohm-m)]
cp	Heat capacity [J/(kmol-K)]
$\dot{E}$	Energy rate [W]
E_a	Arrhenius activation energy [J/kmol]
E_{ocv}	Open circuit voltage [V]
$E_{ocv,0}$	Reversible voltage [V]
F	Faraday's constant [-]
Δg^o	Overall change in Gibbs free energy [J/kmol]
h	Specific enthalpy [kJ/kg]
i	Current density [A/m^2]
i_L	Limiting current density [A/m^2]
I	Current [A]
K	Equilibrium constant [-]
k_o	Arrhenius frequency factor [-]
K_T	Kinetic constant at steady state for WGS reactor [-]
L	Thickness [m]
$\dot{n}$	Molar flow rate [kmol/s]
n_{cell}	Number of cells [-]
n_e	Number of electrons [-]
p	Pressure [Pa]
$\dot{W}$	Power [W]
R	Universal gas constant [J/(kmol-K)]
R_i	Cell resistance [Ohm-m^2]
SC	Steam-to-carbon ratio [-]
$\dot{Q}$	Heat rate [W]
T	Temperature [K]
y	Mole fraction [-]
us_i	Superficial velocity [m/s]
V	Voltage [V]
W	Power density [W/m^2]
w_{amb}	Humidity ratio [-]
U_f	Utilization factor [-]

Greek symbols

α	Symmetry factor [-]
η	Efficiency [-]
λ	Stoichiometry [-]
μ	Viscosity [-]
σ	Ionic or electronic conductivity [1/(Ohm-m)]
ω	Cross-sectional area [m^2]

Subscripts/Superscripts

1, 2, ...	Node number
act	Activation
air	Air
amb	Ambient
ano	Anode
cat	Cathode
cell	Cell
comb	Combustion
con	Consumption
conc	Concentration
ef	Extra fuel
el	Electrical
ele	Electrolyzer
fg	Flue gas
i	In
int	Interconnect
loss	Loss
net	Net amount
o	Out
ohm	Ohmic
pemfc	HT-PEMFC stack
pump	Pump
ref	Pre-reformer
s	Stack
smr	Steam Methane Reformer
sofc	SOFC stack
stoich	Stoichiometric
sup	Supply
wgs	Water Gas Shift

A–b–breviatio–ns

EES	Engineering Equation Solver
HT-PEMFC	High Temperature-Proton Exchange Membrane Fuel Cell
LCC	Lifecycle cost
LHV	Lower Heating Value
PBI	Polybenzimidazole
PEMFC	Proton Exchange Membrane Fuel Cell
SMR	Steam Methane Reformer
SOFC	Solid Oxide Fuel Cell
TSA	Thermal Swing Absorption
WGS	Water Gas Shift

and supplied to the PEMFC subsystem to provide heat to the endothermic reactions of the aforementioned reactor processes (Napoli et al., 2015). In one of the earliest studies (Dicks et al., 2000), the possible advantages of such a system were investigated through simplistic computational simulations. In this configuration, the exhaust flue gas from the SOFC subsystem was directed to shift reactors to generate hydrogen, which was then supplied to a Nafion-based PEMFC. The results of this study identified possible advantages since the system could perform at a higher net electrical efficiency along with a lower fuel consumption. However, the resulting system was significantly complex in terms of overall configuration, due to the high number of integrated reactors. In a later study (Subramanyan et al., 2004), a PEMFC-SOFC system configuration was considered, where the exhaust flue gas from the PEMFC was directed to a combustor and steam generator for further utilization in the total system. The researchers implemented a multi-objective optimization problem and applied a methodology to characterize and quantify uncertainties in the subsystems. The overall aim of this work was to provide a novel integrated approach to hybrid fuel cell systems. In a different study (Tan et al., 2015), a multi-objective optimization under uncertainty for the synthesis/design optimization of a hybrid 220 kW SOFC-PEMFC system was implemented. The study focused on the determination of the effect of uncertainty of key operating variables related to three objectives, namely (a) net electrical efficiency, (b) SOFC current density, and (c) capital cost of the total system. The authors concluded that the objectives are considerably influenced by uncertainties, because the two trade-off surfaces are significantly different.

In a more recent study (Wu et al., 2018), a hybrid PEMFC-SOFC system was considered, where WGS and Thermal Swing Adsorption (TSA) technologies were combined to convert SOFC-generated syngas into hydrogen, with a high purity appropriate for fueling the PEMFC subsystem. The waste heat recovery for driving the TSA reaction and the hydrogen recirculation for the PEMFC were found to further improve the net electrical efficiency. In a subsequent study, the same group (Wu et al., 2019) considered the replacement of the reformer in the generation of hydrogen for the supply of a 300 kW PEMFC vehicle, with an

SOFC subsystem. The results showed that the TSA reactor contributes to the enhanced dynamic response related to the hydrogen supply to the PEMFC subsystem. The power distribution for the hybrid system was 6:4 for the SOFC and PEMFC subsystems, respectively. Later, the authors conducted an economic analysis (Wu et al., 2020) of the hybrid system to maximize the economics of the electricity generation. The specific electricity cost with $LaNi_5$ as the TSA working medium was \$0.04058/kWh, which was significantly lower than that of a conventional system (\$0.0546/kWh). The same research group also considered fueling of the aforementioned system with biogas (Wu et al., 2021a), which resulted in a levelized cost of energy down to \$0.02942/kWh (with subsidies) for a 1 MW system. The same group (Wu et al., 2021b), proposed an SOFC-gas processing-PEMFC system which operates at higher energy and exergy efficiencies than standalone systems at 54.2 % and 66.2 %, respectively. The group also conducted a case study for Northwest China, which showed that the methanol powered system is significantly more cost-efficient than the methanol steam reforming-PEMFC one. Another research group (Yan et al., 2020) proposed a hybrid distributed power generation system with PEMFC and SOFC units, along fuel processing subsystems, with the aim of generating power at the MW scale at high energy efficiency. Different types of fuels were considered, with natural gas and biogas achieving efficiencies at 64 % and 63.5 %, respectively.

A proton conducting SOFC model was modeled in Aspen HYSYS (Milewski et al., 2021). The model was validated with experimental data and an error analysis was subsequently conducted. The model includes several parameters, such as the fuel utilization factor, maximum voltage, and specific resistances. A hybrid system consisting of PEMFC and SOFC subsystems was considered for the production of electricity for an Electric Vehicle charging station (Pourrahmani et al., 2021). The exhaust streams of the two fuel cell units were recovered to operate a Kalina Cycle and an Organic Rankine Cycle (ORC), and therefore generate more power. A methanol-fueled SOFC-PEMFC system was proposed to increase the hybrid system efficiency (Meng et al., 2022). The authors proposed and tested three different system configurations for various applications. The combined combustion system had the highest power production, while the PEMFC water preheating system had the most balanced operation at 300 kW with an efficiency of 66 %. In a very recent study, two hybrid SOFC-PEMFC system configurations were proposed and investigated to increase carbon dioxide capture with minimum performance degradation (Kim et al., 2023). In the first configuration, the PEMFC generates electricity and also carbon capture, while in the second configuration, a pressure swing adsorption is used for carbon dioxide capture. An ORC was added to recover the exhaust heat from the fuel cell units. The results showed that the hybrid system configuration is capable of capturing carbon dioxide very efficiently. In a different study, it was investigated that proper thermal management can improve the efficiency of hydrogen storage chains based on liquid organic hydrogen carriers (Li et al., 2023). Different options for such chains were considered, in terms of both hydrogen generation and hydrogen consumption. Hydrogen consumption included both PEMFC and SOFC units, along with other more conventional engines. The chain with the PEMFC option resulted in the highest energy efficiency, while the SOFC option resulted in the highest exergy efficiency.

It is evident from the aforementioned literature review that so far, proposed hybrid SOFC-PEMFC systems have been rather impractical in terms of system configuration and operational flexibility. A key issue of these systems is the fact that complicated post internal SOFC reforming components are needed to reduce the CO levels at the fuel inlet conditions required by a low temperature PEMFC. The current study attempts to propose and investigate a novel hybrid SOFC—HT-PEMFC system, which has several advantages over more "conventional" hybrid SOFC-PEMFC systems, such as more practical operation, better thermal management, and simpler fuel processing. PBI-based high temperature PEMFC technology is a relatively new technology (in comparison to the more well-established low temperature PEMFC technology) and therefore it has not been considered yet in hybrid fuel cell-to-fuel cell energy system configurations. The overall motivation of this study is to design, model, and optimize a novel 6 kWe hybrid SOFC—HT-PEMFC system. The novelty of this study is the proposal of a completely new hybrid system design, and the inclusion of detailed modeling of all components/subsystems forming the total integrated energy system and an optimization methodology based on genetic algorithms to optimize the proposed energy system in terms of system efficiency, which can lead to improved thermoeconomic performance. The aim is to develop a highly efficient energy system combining two promising fuel cell technologies, while additionally achieving a practical and robust configuration, since HT-PEMFC technology is significantly less demanding in terms of hydrogen purity than low temperature PEMFC technology. Additionally, such a combination is likely to reveal different types of heat recovery, due to the different temperature exhausted from a HT-PEMFC than a Nafion-based PEMFC. In summary, this study includes (a) the design of the hybrid SOFC—HT-PEMFC system configuration, (b) the modeling of the components/subsystem, (c) the integration of the modeled subsystems to the integrated system model, (d) the application of an optimization strategy to optimize system performance, and (e) a cost analysis to investigate the competitiveness of the proposed system. Finally, a case study is conducted to compare the performance of the proposed hybrid SOFC—HT-PEMFC system with standalone SOFC and HT-PEMFC based systems. This is done to help identify possible technical and economic advantages over such standalone systems.

Material and methods

Study methodology

The scientific hypothesis for this work is based on the fact that proposed energy systems must be able to operate efficiently, but within optimum configurations in terms of design and operation (Jaluria, 2008). The merit of a highly efficient system is the fact that it can operate with a minimum fuel consumption and reduced emissions (Arsalis et al., 2012). Therefore a hybrid SOFC—HT-PEMFC system is proposed and chosen for modeling and analysis since SOFC and HT-PEMFC technologies include these important characteristics (Rosli et al., 2019; Wahl et al., 2015). Hybrid systems are generally more complex than standalone systems, and therefore they can only become important candidates in the future energy market, if their design is practical, realistic, and robust (Calise et al., 2017). A Nafion-based PEMFC is highly intolerant to hydrogen that originates from the reforming of natural gas, primarily in terms of the CO content in the incoming hydrogen-rich gas entering the fuel cell anode (Hubert et al., 2006). On the other hand, a PBI-based PEMFC (i.e., HT-PEMFC) is significantly more tolerant to CO contents in the hydrogen-rich mixture, and therefore it can largely eliminate the need for complex CO content reduction, which is needed in Nafion-based PEMFC through post steam reforming fuel processing (i.e., multi-stage WGS reactors, preferential oxidation, etc.) (Arsalis et al., 2011; Büchi et al., 2009).

The mathematical modeling of the total system, including the calculation of all thermophysical properties, the optimization, and the cost analysis are conducted with the commercially available software Engineering Equation Solver (EES) – Professional version (Klein, 2022). Therefore, this software allows a practical and robust way to model, optimize, and analyze the proposed hybrid SOFC—HT-PEMFC system, and also compare it to other existing system configurations. Specifically, this modeling approach allows modeling of each component from first principles, and then combining all subsystems in a total energy system. The developed total energy system is then optimized and analyzed in terms of selected key parameters, such as efficiency and fuel consumption. The proposed system is sized as needed for the comparison to the aforementioned systems and extraction of conclusions on its performance and suitability as an energy solution. In addition to the technical performance of the system, the system is also evaluated in terms of

economic performance. This is done with the development of a cost model and the economic analysis of the proposed system, which includes evaluation of key economic parameters, such as lifecycle cost.

System design and configuration

The first step of this study is the design of the proposed hybrid SOFC—HT-PEMFC system. Since the SOFC unit will perform a dual purpose in the system, i.e., internal reforming of the incoming fuel mixture and generation of electrical energy, it must precede the HT-PEMFC unit in the system configuration. The proposed system also requires several heat exchangers to reduce or increase the temperature of the fluid streams as needed by the operating conditions of each component. For example, the temperatures of the incoming flows of air and fuel to the SOFC unit must be high enough to facilitate its proper operation. The external heat needed is provided by a catalytic combustor integrated in the proposed system. The thermal energy from the combustor is distributed at the temperature levels needed through connections to the various components starting from the pre-reformer (steam methane reformer), which requires external heating for the endothermic reaction that generates a hydrogen-rich gas. The heat exiting the pre-reformer is then distributed to other components, to perform internal system tasks, such as natural gas preheating, air preheating for the SOFC cathode inlet, and water preheating to generate steam for the pre-reformer. Additionally, the temperature of the exiting mixture flow from the SOFC must be reduced at the level necessary for the WGS reactor, and similarly the temperature of the exiting hydrogen-rich mixture from the WGS reactor must be reduced further to reach the operating temperature of the PEMFC unit. Therefore, these processes require cooling through streams that are at a lower temperature; in this case this cooling supply originates from the PEMFC exhaust stream.

In the proposed hybrid SOFC—HT-PEMFC system, shown in Fig. 1, natural gas passes through the desulfurizer, and then through heat exchanger H1 for preheating. Water from the water tank is pumped with the water pump to heat exchanger H2 (steam generator). Natural gas and steam are pre-mixed though the mixer and then directed to the pre-reformer, which receives heat from the combustor to generate hydrogen-rich syngas. The syngas is supplied to the SOFC stack to generate electricity. The excess syngas exiting the SOFC stack is directed to heat exchanger H4 and then to the WGS reactor, which decreases the CO content in the mixture to a level acceptable for the HT-PEMFC stack. The hydrogen-rich gas exiting the WGS reactor must pass through heat exchanger H5 to reduce its temperature down to the operating temperature of the HT-PEMFC stack. The excess air exiting the SOFC stack is directed to the combustor. The exhaust mixture exiting the HT-PEMFC passes through heat exchangers H5, H4 and H6, and finally it is directed to the combustor. Additional natural gas can be supplied to the combustor as needed. The flue gas stream exiting the pre-reformer is split into two flows; one flow is directed to H6 and the other to H3 (to preheat the air for the SOFC stack). The two flue gas streams are unified in a mixer, and water from the flue gas mixture is recovered through a water separator and then returned to the water tank. The values of the constant parameters in this study are tabulated in Table 1. For the purpose of comparing the performance of the proposed hybrid SOFC—HT-PEMFC system, two standalone fuel cell system configurations are also considered, namely an SOFC-based system (shown in Fig. 2), and an HT-PEMFC-based system (shown in Fig. 3).

The following design and modeling assumptions have been made for this study:

(1) For calculation simplicity, natural gas is assumed to have the same thermophysical properties as methane.
(2) To improve the net electrical efficiency, the utilization of flue gas is maximized with the addition of a bypass valve after node 15, which splits the flue gas flow to nodes 28 & 29.

Table 1
Values of the constant parameters in the proposed hybrid solid oxide fuel cell—high temperature-proton exchange membrane fuel cell system.

Parameter	Description	Value
p_{amb}	Ambient pressure	1 atm
T_{amb}	Ambient temperature	25 °C
T_{sofc}	SOFC operating temperature	750 °C
T_{pemfc}	HT-PEMFC operating temperature	160 °C
T_1	Temperature of natural gas supply	15 °C
T_4	Temperature of natural gas at H1 exit	450 °C
T_8	Temperature of syngas at H4 exit	250 °C

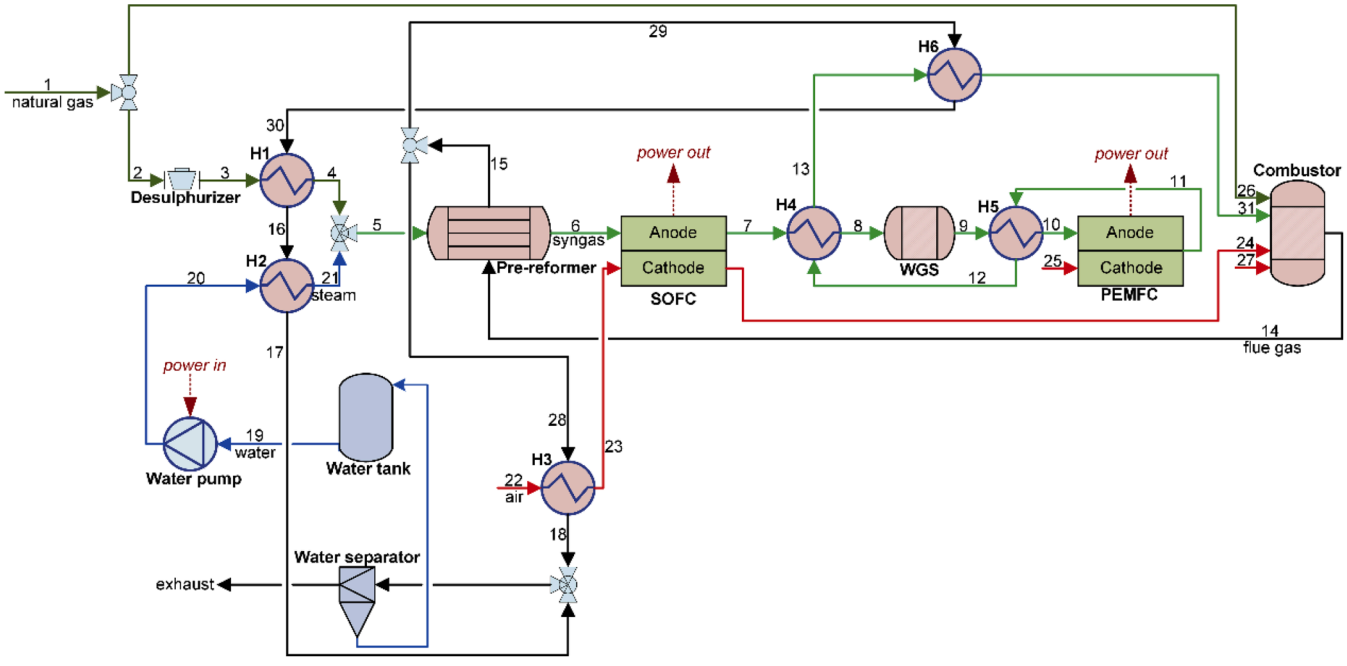

Fig. 1. Schematic representation of the proposed hybrid solid oxide fuel cell—high temperature-proton exchange membrane fuel cell system.

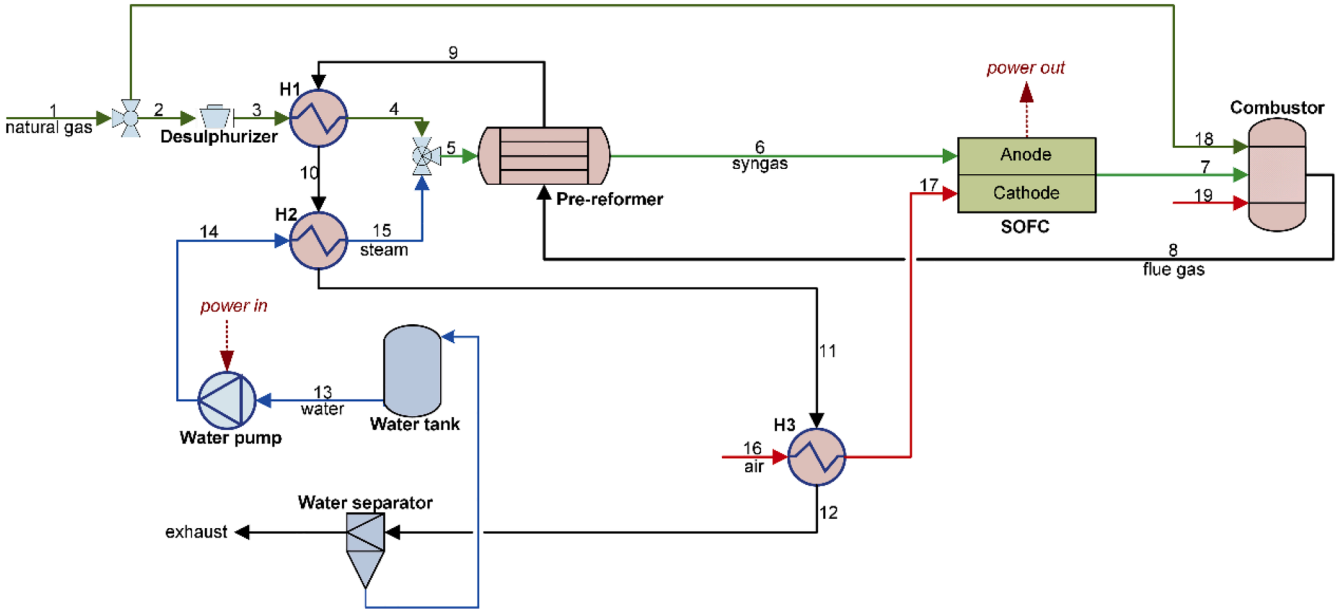

Fig. 2. Schematic representation of the standalone Solid Oxide Fuel Cell-based system.

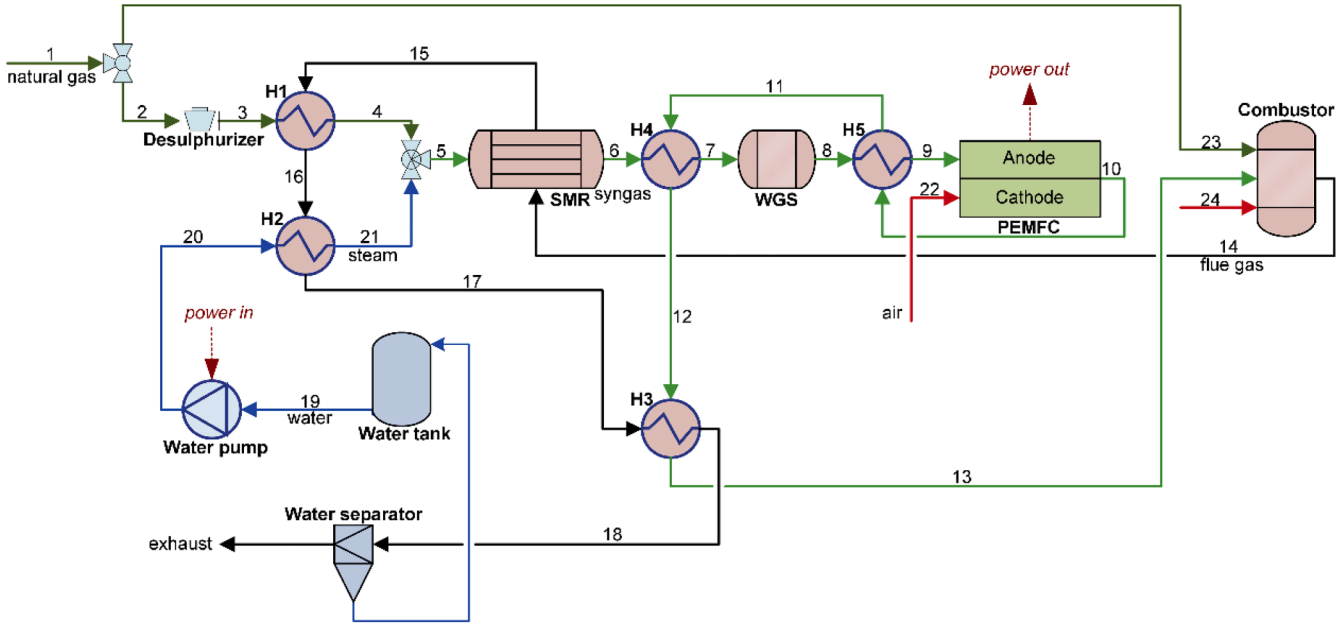

Fig. 3. Schematic representation of the standalone High Temperature-Proton Exchange Membrane Fuel Cell based system.

(3) A heat exchanger (H6) is integrated in the system configuration to allow heating of the HT-PEMFC exhaust flow, before feeding it to the combustor.
(4) Heat losses at a fixed percentage of 3 % have been considered for the pre-reformer, the SOFC, the HT-PEMFC, and the combustor.
(5) Pressure losses at a fixed value of 1000 Pa have been considered for the desulfurizer, the heat exchangers, the SOFC, the WGS, the HT-PEMFC, the combustor, and the pre-reformer.
(6) In terms of modeling limitations, a zero-dimensional, steady state model has been adopted. Therefore, the dynamic behavior of the proposed system has not been considered in this study.

System modeling

This section provides a description of the modeling details of the system, starting with a description of the modeling for every component (pre-reformer, WGS reactor, SOFC, HT-PEMFC, combustor, and auxiliary components). Subsequently, the definitions of energy and efficiency for the total system are provided. Finally, the details of the system optimization and the cost model are given.

Pre-reformer

The pre-reformer model is based on a chemical equilibrium Steam Methane Reformer (SMR) reactor model (Calise et al., 2006a). The

model considers both the methane-steam and WGS reactions:

$$CH_4 + H_2O \rightarrow CO + 3H_2 \quad (1)$$

$$CO + H_2O \rightarrow CO_2 + H_2 \quad (2)$$

The following equations allow calculation of the equilibrium constants at the given temperature for the methane-steam and WGS reactions, respectively:

$$K_{smr} = \exp\left(\frac{-\Delta g^{o}_{smr}}{RT_{ref,o}}\right) \quad (3)$$

$$K_{wgs} = \exp\left(\frac{-\Delta g^{o}_{wgs}}{RT_{ref,o}}\right) \quad (4)$$

Δg^{o}_{smr}, Δg^{o}_{wgs} are the overall change in Gibbs free energy for the methane-steam and WGS reactions, respectively, R is the universal gas constant, and $T_{ref,o}$ is the pre-reformer exit temperature.

The equations related to the reformate at the inlet are the following:

$$y_{ref,i,CH4} + y_{ref,i,H2O} = 1 \quad (5)$$

$$y_{ref,i,H2O} = y_{ref,i,CH4} SC \quad (6)$$

$$\dot{n}_{ref,i,CH4} = y_{ref,i,CH4} \dot{n}_{ref,i} \quad (7)$$

$$\dot{n}_{ref,i,H2O} = y_{ref,i,H2O} \dot{n}_{ref,i} \quad (8)$$

$y_{ref,i,CH4}$, $y_{ref,i,H2O}$ are the methane and water mole fractions of the reformate at the inlet, respectively. SC is the steam-to-carbon ratio. $\dot{n}_{ref,i,CH4}$ and $\dot{n}_{ref,i,H2O}$ are the molar flow rates of methane and water of the reformate at the inlet, respectively. $\dot{n}_{ref,i}$is the total molar flow rate of the reformate at the inlet of the pre-reformer.

Mass balances are set between the inlet and exit flows to determine the change of all species at the pre-reformer exit:

$$\dot{n}_{ref,o,CH4} = \dot{n}_{ref,i,CH4} - \dot{x} \quad (9)$$

$$\dot{n}_{ref,o,H2O} = \dot{n}_{ref,i,H2O} - \dot{x} - \dot{y} \quad (10)$$

$$\dot{n}_{ref,o,CO} = \dot{x} - \dot{y} \quad (11)$$

$$\dot{n}_{ref,o,H2} = 3\dot{x} + \dot{y} \quad (12)$$

$$\dot{n}_{ref,o,CO2} = \dot{y} \quad (13)$$

$$\dot{n}_{ref,o} = \dot{n}_{ref,i,CH4} + \dot{n}_{ref,i,H2O} + 2\dot{x} \quad (14)$$

$\dot{n}_{ref,o,CH4}$, $\dot{n}_{ref,o,H2O}$, $\dot{n}_{ref,o,CO}$, $\dot{n}_{ref,o,H2}$ and $\dot{n}_{ref,o,CO2}$are the molar flow rates of methane, water, carbon monoxide, hydrogen, and carbon dioxide of the reformate at the exit, respectively. $\dot{n}_{ref,o}$is the total molar flow rate of the reformate at the exit of the pre-reformer.

The mole fractions at the exit of the pre-reformer can be determined with the mole fraction definitions, and equilibrium constant relations can be defined in relation to the mole fractions at the pre-reformer exit, as follows:

$$\dot{n}_{ref,o,CH4} = y_{ref,o,CH4} \dot{n}_{ref,o} \quad (15)$$

$$\dot{n}_{ref,o,H2O} = y_{ref,o,H2O} \cdot \dot{n}_{ref,o} \quad (16)$$

$$\dot{n}_{ref,o,CO} = y_{ref,o,CO} \dot{n}_{ref,o} \quad (17)$$

$$\dot{n}_{ref,o,H2} = y_{ref,o,H2} \dot{n}_{ref,o} \quad (18)$$

$$\dot{n}_{ref,o,CO2} = y_{ref,o,CO2} \dot{n}_{ref,o} \quad (19)$$

$$K_{smr} = \frac{y_{ref,o,CO} y_{ref,o,H2}{}^{3}}{y_{ref,o,CH4} y_{ref,o,H2O}} \left(\frac{p_{ref,o}}{p_{amb}}\right)^{2} \quad (20)$$

$$K_{wgs} = \frac{y_{ref,o,CO2} y_{ref,o,H2}}{y_{ref,o,CO} y_{ref,o,H2O}} \quad (21)$$

$y_{ref,o,CH4}$, $y_{ref,o,H2O}$, $y_{ref,o,CO}$, $y_{ref,o,H2}$ and $y_{ref,o,CO2}$ are the mole fractions of the reformate at the exit of the pre-reformer for methane, water, carbon monoxide, hydrogen, and carbon dioxide, respectively. $p_{ref,o}$, p_{amb} are the reformate pressure at the exit of the pre-reformer and the ambient pressure, respectively.

Finally, an energy balance can be set to relate the energy input, energy output and heat addition to the pre-reformer:

$$\dot{E}_{i,smr} = \dot{n}_{ref,i,CH4} h_{ref,i,CH4} + \dot{n}_{ref,i,H2O} h_{ref,i,H2O} \quad (22)$$

$$\dot{E}_{o,smr} = \dot{n}_{ref,o,CH4} h_{ref,o,CH4} + \dot{n}_{ref,o,H2O} h_{ref,o,H2O} + \dot{n}_{ref,o,CO} h_{ref,o,CO} + \dot{n}_{ref,o,H2} h_{ref,o,H2} + \dot{n}_{ref,o,CO2} h_{ref,o,CO2} \quad (23)$$

$$\dot{Q}_{heat,smr} = \dot{n}_{fg,O2}\left(h_{fg,O2,i} - h_{fg,O2,o}\right) + \dot{n}_{fg,N2}\left(h_{fg,N2,i} - h_{fg,N2,o}\right) + \dot{n}_{fg,CO2}\left(h_{fg,CO2,i} - h_{fg,CO2,o}\right) + \dot{n}_{fg,H2O}\left(h_{fg,H2O,i} - h_{fg,H2O,o}\right) \quad (24)$$

$$\dot{Q}_{heat,smr} + \dot{E}_{i,smr} = \dot{E}_{o,smr} + \dot{Q}_{loss,smr} \quad (25)$$

$\dot{E}_{i,smr}$, $\dot{E}_{o,smr}$ are the reformate energy at the inlet and exit of the pre-reformer, respectively. $\dot{Q}_{heat,smr}$, $\dot{Q}_{loss,smr}$ are the heat addition to the pre-reformer and the heat loss, respectively. $h_{ref,i,CH4}$, $h_{ref,i,H2O}$ are the specific enthalpies of methane and water for the reformate at the inlet of the pre-reformer. $h_{ref,o,CH4}$, $h_{ref,o,H2O}$, $h_{ref,o,CO}$, $h_{ref,o,H2}$ and $h_{ref,o,CO2}$ are the specific enthalpies for methane, water, carbon monoxide, hydrogen and carbon dioxide for the reformate at the exit of the pre-reformer, respectively. $\dot{n}_{fg,O2}$, $\dot{n}_{fg,N2}$, $\dot{n}_{fg,CO2}$ and $\dot{n}_{fg,H2O}$ are the molar flow rate of the hot flue gas for oxygen, nitrogen, carbon dioxide and water, respectively. $h_{fg,O2,i}$, $h_{fg,O2,o}$ are the flue gas specific enthalpies of oxygen at the inlet and exit, respectively. $h_{fg,N2,i}$, $h_{fg,N2,o}$ are the flue gas specific enthalpies of nitrogen at the inlet and exit, respectively. $h_{fg,CO2,i}$, $h_{fg,CO2,o}$ are the flue gas specific enthalpies of carbon dioxide at the inlet and exit, respectively. $h_{fg,H2O,i}$, $h_{fg,H2O,o}$ are the flue gas specific enthalpies of water at the inlet and exit, respectively.

WGS reactor

The WGS reactor considers the exothermic chemical reaction given in Eq. (2). The equilibrium constant is defined as a function of temperature, as follows (Davies and Lihou, 1971):

$$K_T = \exp\left(\frac{4400}{T_{o,wgs}} - 4.063\right) \quad (26)$$

$T_{o,wgs}$is the temperature of the reformate at the WGS reactor exit.

The WGS reaction rate equations are defined as follows (Keiski et al., 1996):

$$K_{wgs,2} = k_o \exp\left(-\frac{E_a}{RT_{o,wgs}}\right) \quad (27)$$

$$\beta = \frac{c_{o,CO_2} c_{o,H_2}}{K_T c_{o,CO} c_{o,H_2O}} \quad (28)$$

$$r_{CO} = K_{wgs,2} c_{o,CO}{}^{n} c_{o,H2O}{}^{m} c_{o,CO2}{}^{p} c_{o,H2}{}^{q} (1-\beta) \quad (29)$$

k_o is the Arrhenius frequency factor, E_a is the Arrhenius activation energy, β is the reversibility factor, and r_{CO} is the reaction rate. $c_{o,CO}$, $c_{o,H2O}$, $c_{o,CO2}$ and $c_{o,H2}$ are the exit molar concentrations for carbon monoxide, water, carbon dioxide, and hydrogen, respectively. n, m, p and q are the concentration exponents for carbon monoxide, water, carbon dioxide, and hydrogen, respectively.

The superficial velocities at the inlet and exit are defined as follows,

respectively:

$$us_{\mathrm{i}} = \left(\frac{\dot{n}_{\mathrm{i}}}{\omega}\right) R \left(\frac{T_{\mathrm{i}}}{p_{\mathrm{i}}}\right) \tag{30}$$

$$us_{\mathrm{o}} = us_{\mathrm{i}} \left(\frac{T_{\mathrm{o}}}{T_{\mathrm{i}}}\right) \tag{31}$$

ω is the cross-sectional area. T_{i},p_{i},$\dot{n}_{\mathrm{i}}$are the temperature, pressure, and molar flow rate at the WGS reactor inlet. T_{o} is the temperature at the WGS reactor exit.

The average mixture viscosity at the exit is given as follows:

$$\mu_{\mathrm{o}} = \frac{p_{\mathrm{o,CH4}}\mu_{\mathrm{o,CH4}} + p_{\mathrm{o,CO2}}\mu_{\mathrm{o,CO2}} + p_{\mathrm{o,H2O}}\mu_{\mathrm{o,H2O}} + p_{\mathrm{o,CO}}\mu_{\mathrm{o,CO}} + p_{\mathrm{o,H2}}\mu_{\mathrm{o,H2}}}{p_{\mathrm{i}}} \tag{32}$$

$p_{\mathrm{o,CH4}}$, $p_{\mathrm{o,CO2}}$, $p_{\mathrm{o,H2O}}$, $p_{\mathrm{o,CO}}$ and $p_{\mathrm{o,H2}}$ are the partial pressures at the exit for methane, carbon dioxide, water, carbon monoxide, and hydrogen, respectively. $\mu_{\mathrm{o,CH4}}$, $\mu_{\mathrm{o,CO2}}$, $\mu_{\mathrm{o,H2O}}$, $\mu_{\mathrm{o,CO}}$ and $\mu_{\mathrm{o,H2}}$ are the viscosities at the exit for methane, carbon dioxide, water, carbon monoxide, and hydrogen, respectively.

The average mixture heat capacity at the exit is given as follows:

$$cp_{\mathrm{o}} = \frac{p_{\mathrm{o,CH4}}cp_{\mathrm{o,CH4}} + p_{\mathrm{o,CO2}}cp_{\mathrm{o,CO2}} + p_{\mathrm{o,H2O}}cp_{\mathrm{o,H2O}} + p_{\mathrm{o,CO}}cp_{\mathrm{o,CO}} + p_{\mathrm{o,H2}}cp_{\mathrm{o,H2}}}{p_{\mathrm{i}}} \tag{33}$$

$cp_{\mathrm{o,CH4}}$, $cp_{\mathrm{o,CO2}}$, $cp_{\mathrm{o,H2O}}$, $cp_{\mathrm{o,CO}}$ and $cp_{\mathrm{o,H2}}$ are the heat capacities at the exit for methane, carbon dioxide, water, carbon monoxide, and hydrogen, respectively.

Finally, an energy balance is performed in the WGS reactor:

$$E_{\mathrm{i,wgs}} = \dot{n}_{\mathrm{i,CH4}}h_{\mathrm{i,CH4}} + \dot{n}_{\mathrm{i,CO2}}h_{\mathrm{i,CO2}} + \dot{n}_{\mathrm{i,CO}}h_{\mathrm{i,CO}} + \dot{n}_{\mathrm{i,H2}}h_{\mathrm{i,H2}} + \dot{n}_{\mathrm{i,H2O}}h_{\mathrm{i,H2O}} \tag{34}$$

$$E_{\mathrm{o,wgs}} = \dot{n}_{\mathrm{o,CH4}}h_{\mathrm{o,CH4}} + \dot{n}_{\mathrm{o,CO2}}h_{\mathrm{o,CO2}} + \dot{n}_{\mathrm{o,CO}}h_{\mathrm{o,CO}} + \dot{n}_{\mathrm{o,H2}}h_{\mathrm{o,H2}} + \dot{n}_{\mathrm{o,H2O}}h_{\mathrm{o,H2O}} \tag{35}$$

$$\Delta E_{\mathrm{wgs}} = E_{\mathrm{o,wgs}} - E_{\mathrm{i,wgs}} \tag{36}$$

SOFC

The SOFC model considers the fuel cell reaction:

$$2H_2 + O_2 \rightarrow 2H_2O \tag{37}$$

The model is based on planar SOFC technology and in addition to the aforementioned fuel cell reaction, it also considers the internal SMR and the WGS reforming reactions at chemical equilibrium. Changes in thermodynamic and electrochemical properties are assumed to be negligible along the fuel cell. Also, the fuel cell temperature and pressure are set to be constant throughout the fuel cell since the exiting radial temperature gradients are negligible. The process for determining the equilibrium constants for the SMR and the WGS reactions is identical to the description of the pre-reformer model (see above description).

The reversible voltage can be calculated as follows (Calise et al., 2006a):

$$E_{\mathrm{ocv},0} = \frac{-\Delta g^{\mathrm{o}}_{\mathrm{f}}}{n_{\mathrm{e}}F} \tag{38}$$

$\Delta g^{\mathrm{o}}_{\mathrm{f}}$ is the overall change in Gibbs free energy for the fuel cell reaction, n_{e} is the number of electrons transferred per hydrogen molecule reacted, and F is the Faraday's constant.

For the fuel cell reaction, the open circuit voltage is determined as follows (Larminie and Dicks, 2003):

$$E_{\mathrm{ocv}} = E_{\mathrm{ocv},0} + \frac{RT_{\mathrm{s}}}{2F}\ln\left(\frac{\frac{y_{\mathrm{ano,H2}}p_{\mathrm{s}}}{p_{\mathrm{amb}}}\sqrt{\frac{y_{\mathrm{cat,O2}}p_{\mathrm{s}}}{p_{\mathrm{amb}}}}}{\frac{y_{\mathrm{ano,H2O}}p_{\mathrm{s}}}{p_{\mathrm{amb}}}}\right) \tag{39}$$

p_{s}, T_{s} are the SOFC stack pressure and temperature, respectively. $y_{\mathrm{ano,H2}}$ is the hydrogen mole fraction at the anode, $y_{\mathrm{cat,O2}}$ is the oxygen mole fraction at the cathode, and $y_{\mathrm{ano,H2O}}$is the water mole fraction at the anode. The mole fractions are calculated with average values between the inlet and the exit of the anode and the cathode.

The activation losses can be calculated using the Butler-Volmer equation (Zhao et al., 2011). They are the sum of the activation losses in the anode and the cathode:

$$V_{\mathrm{act,ano}} = \frac{2RT_{\mathrm{s}}}{n_{\mathrm{e}}F}\operatorname{arcsinh}\left(\frac{i}{2i_{0,\mathrm{ano}}}\right) \tag{40}$$

$$V_{\mathrm{act,cat}} = \frac{2RT_{\mathrm{s}}}{n_{\mathrm{e}}F}\operatorname{arcsinh}\left(\frac{i}{2i_{0,\mathrm{cat}}}\right) \tag{41}$$

$$V_{\mathrm{act}} = V_{\mathrm{act,ano}} + V_{\mathrm{act,cat}} \tag{42}$$

i is the current density, $i_{0,\mathrm{ano}}$ is the anode exchange current density, and $i_{0,\mathrm{cat}}$ is the cathode exchange current density.

The Ohmic losses can be calculated as follows (Zhao et al., 2011):

$$V_{\mathrm{ohm}} = i\left(\frac{L_{\mathrm{ele}}}{\sigma_{\mathrm{ele}}} + \frac{L_{\mathrm{ano}}}{\sigma_{\mathrm{ano}}} + \frac{L_{\mathrm{cat}}}{\sigma_{\mathrm{cat}}} + \frac{L_{\mathrm{int}}}{\sigma_{\mathrm{int}}}\right) \tag{43}$$

L_{ele}, L_{ano}, L_{cat}, L_{int} are the thicknesses for the electrolyte, the anode, the cathode, and the interconnect, respectively.

σ_{ele}, σ_{ano}, σ_{cat}, and σ_{int} are the ionic conductivity of the electrolyzer, the electronic conductivity of the anode, the electronic conductivity of the cathode, and the electronic conductivity of the interconnect, respectively. They are determined as follows:

$$\sigma_{\mathrm{ele}} = (C_{1,\mathrm{ele}})\exp\left(\frac{C_{2,\mathrm{ele}}}{T_s}\right) \tag{44}$$

$$\sigma_{\mathrm{ano}} = \left(\frac{C_{1,\mathrm{ano}}}{T_{\mathrm{s}}}\right)\exp\left(\frac{C_{2,\mathrm{ano}}}{T_{\mathrm{s}}}\right) \tag{45}$$

$$\sigma_{\mathrm{cat}} = \left(\frac{C_{1,\mathrm{cat}}}{T_{\mathrm{s}}}\right)\exp\left(\frac{C_{2,\mathrm{cat}}}{T_{\mathrm{s}}}\right) \tag{46}$$

$$\sigma_{\mathrm{int}} = \left(\frac{C_{1,\mathrm{int}}}{T_{\mathrm{s}}}\right)\exp\left(\frac{C_{2,\mathrm{int}}}{T_{\mathrm{s}}}\right) \tag{47}$$

$C_{1,\mathrm{ele}}$, $C_{2,\mathrm{ele}}$ are the electrolyte conductivity constants; $C_{1,\mathrm{ano}}$, $C_{2,\mathrm{ano}}$ are the anode conductivity constants; $C_{1,\mathrm{cat}}$, $C_{2,\mathrm{cat}}$ are the cathode conductivity constants; and $C_{1,\mathrm{int}}$, $C_{2,\mathrm{int}}$ are the interconnect conductivity constants.

Concentration losses are the incremental voltage losses due to reactant depletion in the catalyst layer, and can be determined as the difference between the Nernst potential at the catalyst layer and the bulk flow at both the anode and the cathode (Zhao et al., 2011):

$$V_{\mathrm{conc,ano}} = -\frac{RT_{\mathrm{s}}}{n_{\mathrm{e}}F}\ln\left(1 - \frac{i}{i_{\mathrm{L,ano}}}\right) \tag{48}$$

$$V_{\mathrm{conc,cat}} = -\frac{RT_{\mathrm{s}}}{n_{\mathrm{e}}F}\ln\left(1 - \frac{i}{i_{\mathrm{L,cat}}}\right) \tag{49}$$

$$V_{\mathrm{conc}} = V_{\mathrm{conc,ano}} + V_{\mathrm{conc,cat}} \tag{50}$$

$i_{\mathrm{L,ano}}$ and $i_{\mathrm{L,cat}}$ are the limiting current densities in the anode and the cathode, respectively.

The cell voltage, the power density, and the stack voltage are determined as follows, respectively:

$$V_{\mathrm{cell}} = E_{\mathrm{ocv}} - (V_{\mathrm{act}} + V_{\mathrm{ohm}} + V_{\mathrm{conc}}) \tag{51}$$

$$W_{\mathrm{cell}} = V_{\mathrm{cell}}i \tag{52}$$

$$V_s = V_{cell} n_{cell} \tag{53}$$

V_{cell} is the cell voltage, and n_{cell} is the number of cells.

Then, the stack power output and the stack current can be determined:

$$\dot{W}_{sofc} = A_s n_{cell} W_{cell} \tag{54}$$

$$I_s = \frac{\dot{W}_{sofc}}{V_s} \tag{55}$$

A_s is the fuel cell active area and $\dot{W}_{sofc}$ is the SOFC power output.

The hydrogen consumption molar flow rate is determined as follows:

$$\dot{n}_{con,H2} = I_s \frac{n_{cell}}{n_e F} \tag{56}$$

To calculate the partial molar flow rates at the anode exit, the following relations for each species can be defined (Calise et al., 2007):

$$\dot{z} = \dot{n}_{con,H2} \tag{57}$$

$$\dot{n}_{ano,o,CH4} = \dot{n}_{ano,i,CH4} - \dot{x} \tag{58}$$

$$\dot{n}_{ano,o,H2O} = \dot{n}_{ano,i,H2O} - \dot{x} - \dot{y} + \dot{z} \tag{59}$$

$$\dot{n}_{ano,o,CO} = \dot{n}_{ano,i,CO} + \dot{x} - \dot{y} \tag{60}$$

$$\dot{n}_{ano,o,H2} = \dot{n}_{ano,i,H2} + 3\dot{x} + \dot{y} - \dot{z} \tag{61}$$

$$\dot{n}_{ano,o,CO2} = \dot{n}_{ano,i,CO2} + \dot{y} \tag{62}$$

$$\dot{n}_{ano,o} = \dot{n}_{ano,i} + 2\dot{x} \tag{63}$$

$\dot{n}_{ano,i,CH4}$, $\dot{n}_{ano,i,H2O}$, $\dot{n}_{ano,i,CO}$, $\dot{n}_{ano,i,H2}$, and $\dot{n}_{ano,i,CO2}$ are the molar flow rates at the anode inlet for methane, water, carbon monoxide, hydrogen, and carbon dioxide, respectively. $\dot{n}_{ano,i}$ is the total molar flow rate of the mixture at the anode inlet.

$\dot{n}_{ano,o,CH4}$, $\dot{n}_{ano,o,H2O}$, $\dot{n}_{ano,o,CO}$, $\dot{n}_{ano,o,H2}$, and $\dot{n}_{ano,o,CO2}$ are the molar flow rates at the anode exit for methane, water, carbon monoxide, hydrogen, and carbon dioxide, respectively. $\dot{n}_{ano,o}$ is the total molar flow rate of the mixture at the anode exit.

The equilibrium constants for the SMR and the WGS reactions are determined as follows, respectively:

$$K_{smr,SOFC} = \frac{\dot{n}_{ano,o,CO} \dot{n}_{ano,o,H2}{}^3}{\dot{n}_{ano,o,CH4} \dot{n}_{ano,o,H2O} \dot{n}_{ano,o}{}^2} \left(\frac{p_s}{p_{amb}} \right)^2 \tag{64}$$

$$K_{wgs,SOFC} = \frac{\dot{n}_{ano,o,CO2} \dot{n}_{ano,o,H2}}{\dot{n}_{ano,o,CO} \dot{n}_{ano,o,H2O}} \tag{65}$$

The utilization factor is determined as follows:

$$U_f = \frac{\dot{z}}{\dot{n}_{ano,i,H2} + 3\dot{x} + \dot{y}} \tag{66}$$

The molar flow rates for oxygen consumption, water generation, and hydrogen supply are determined as follows, respectively:

$$\dot{n}_{con,O2} = 0.5\dot{z} \tag{67}$$

$$\dot{n}_{gen,H2O} = \dot{z} \tag{68}$$

$$\dot{n}_{sup,H2} = \dot{n}_{ano,i,H2} + 3\dot{x} + \dot{y} \tag{69}$$

The anode and cathode stoichiometries are related to the hydrogen and the air (oxygen) content, respectively:

$$\lambda_{ano} = \frac{\dot{n}_{sup,H2}}{\dot{n}_{con,H2}} \tag{70}$$

$$\lambda_{cat} = \frac{\dot{n}_{cat,i,O2}}{\dot{n}_{con,O2}} \tag{71}$$

$\dot{n}_{cat,i,O2}$ is the molar flow rate of oxygen at the cathode inlet.

To perform an energy balance in the SOFC stack, the mole fractions in the cathode and anode inlets and exits must be determined.

In the cathode inlet:

$$\dot{n}_{cat,i,N2} = 3.76\dot{n}_{cat,i,O2} \tag{72}$$

$$\dot{n}_{cat,i} = \dot{n}_{cat,i,O2} + \dot{n}_{cat,i,N2} \tag{73}$$

$$y_{cat,i,O2} = \frac{\dot{n}_{cat,i,O2}}{\dot{n}_{cat,i}} \tag{74}$$

$$y_{cat,i,N2} = \frac{\dot{n}_{cat,i,N2}}{\dot{n}_{cat,i}} \tag{75}$$

$\dot{n}_{cat,i,N2}$ is the molar flow rate of nitrogen at the cathode inlet. $\dot{n}_{cat,i}$ is the total molar flow rate in the cathode inlet. $y_{cat,i,O2}$ and $y_{cat,i,N2}$ are the mole fractions in the cathode inlet for oxygen and nitrogen, respectively.

In the cathode exit:

$$\dot{n}_{cat,o,O2} = \dot{n}_{cat,i,O2} - \dot{n}_{con,O2} \tag{76}$$

$$\dot{n}_{cat,o,N2} = \dot{n}_{cat,i,N2} \tag{77}$$

$$\dot{n}_{cat,o} = \dot{n}_{cat,o,O2} + \dot{n}_{cat,o,N2} \tag{78}$$

$$y_{cat,o,O2} = \frac{\dot{n}_{cat,o,O2}}{\dot{n}_{cat,o}} \tag{79}$$

$$y_{cat,o,N2} = \frac{\dot{n}_{cat,o,N2}}{\dot{n}_{cat,o}} \tag{80}$$

$\dot{n}_{cat,o,O2}$ and $\dot{n}_{cat,o,N2}$ are the molar flow rates in the cathode exit for oxygen and nitrogen, respectively. $\dot{n}_{cat,o}$ is the total molar flow rate at the cathode exit. $y_{cat,o,O2}$ and $y_{cat,o,N2}$ are the mole fractions in the cathode inlet for oxygen and nitrogen, respectively.

In the anode inlet:

$$\dot{n}_{ano,i,H2} = y_{ano,i,H2} \dot{n}_{ano,i} \tag{81}$$

$$\dot{n}_{ano,i,H2O} = y_{ano,i,H2O} \dot{n}_{ano,i} \tag{82}$$

$$\dot{n}_{ano,i,CO} = y_{ano,i,CO} \dot{n}_{ano,i} \tag{83}$$

$$\dot{n}_{ano,i,CO2} = y_{ano,i,CO2} \dot{n}_{ano,i} \tag{84}$$

$$\dot{n}_{ano,i,CH4} = y_{ano,i,CH4} \dot{n}_{ano,i} \tag{85}$$

$y_{ano,i,H2}$, $y_{ano,i,H2O}$, $y_{ano,i,CO}$, $y_{ano,i,CO2}$, and $y_{ano,i,CH4}$ are the mole fractions at the anode inlet for hydrogen, water, carbon monoxide, carbon dioxide, and methane, respectively.

In the anode exit:

$$y_{ano,o,H2} = \frac{\dot{n}_{ano,o,H2}}{\dot{n}_{ano,o}} \tag{86}$$

$$y_{ano,o,H2O} = \frac{\dot{n}_{ano,o,H2O}}{\dot{n}_{ano,o}} \tag{87}$$

$$y_{ano,o,CO} = \frac{\dot{n}_{ano,o,CO}}{\dot{n}_{ano,o}} \tag{88}$$

$$y_{ano,o,CO2} = \frac{\dot{n}_{ano,o,CO2}}{\dot{n}_{ano,o}} \tag{89}$$

$$y_{ano,o,CH4} = \frac{\dot{n}_{ano,o,CH4}}{\dot{n}_{ano,o}} \tag{90}$$

$y_{ano,o,H2}$, $y_{ano,o,H2O}$, $y_{ano,o,CO}$, $y_{ano,o,CO2}$, and $y_{ano,o,CH4}$ are the mole fractions at the anode exit for hydrogen, water, carbon monoxide, carbon dioxide,

and methane, respectively.

Finally, an energy balance can be performed on the SOFC to determine the required oxygen supply molar flow rate in the cathode. The energy at the inlet and the exit of the SOFC are determined as follows, respectively:

$$\dot{Q}_{\mathrm{i,sofc}} = \dot{n}_{\mathrm{ano,i,CH4}} h_{\mathrm{ano,i,CH4}} + \dot{n}_{\mathrm{ano,i,H2O}} h_{\mathrm{ano,i,H2O}} + \dot{n}_{\mathrm{ano,i,CO}} h_{\mathrm{ano,i,CO}} + \dot{n}_{\mathrm{ano,i,H2}} h_{\mathrm{ano,i,H2}} + \dot{n}_{\mathrm{ano,i,CO2}} h_{\mathrm{ano,i,CO2}} + \dot{n}_{\mathrm{cat,i,O2}} h_{\mathrm{cat,i,O2}} + \dot{n}_{\mathrm{cat,i,N2}} h_{\mathrm{cat,i,N2}} \quad (91)$$

$$\dot{Q}_{\mathrm{o,sofc}} = \dot{n}_{\mathrm{ano,o,CH4}} h_{\mathrm{ano,o,CH4}} + \dot{n}_{\mathrm{ano,o,H2O}} h_{\mathrm{ano,o,H2O}} + \dot{n}_{\mathrm{ano,o,CO}} h_{\mathrm{ano,o,CO}} + \dot{n}_{\mathrm{ano,o,H2}} h_{\mathrm{ano,o,H2}} + \dot{n}_{\mathrm{ano,o,CO2}} h_{\mathrm{ano,o,CO2}} + \dot{n}_{\mathrm{cat,o,O2}} h_{\mathrm{cat,o,O2}} + \dot{n}_{\mathrm{cat,o,N2}} h_{\mathrm{cat,o,N2}} \quad (92)$$

$h_{\mathrm{ano,i,CH4}}$, $h_{\mathrm{ano,i,H2O}}$, $h_{\mathrm{ano,i,CO}}$, $h_{\mathrm{ano,i,H2}}$, and $h_{\mathrm{ano,i,CO2}}$ are the specific enthalpies in the anode inlet for methane, water, carbon monoxide, hydrogen, and carbon dioxide, respectively. $h_{\mathrm{cat,i,O2}}$, and $h_{\mathrm{cat,i,N2}}$ are the specific enthalpies at the cathode inlet for oxygen and nitrogen, respectively.

$h_{\mathrm{ano,o,CH4}}$, $h_{\mathrm{ano,o,H2O}}$, $h_{\mathrm{ano,o,CO}}$, $h_{\mathrm{ano,o,H2}}$, and $h_{\mathrm{ano,o,CO2}}$ are the specific enthalpies in the anode exit for methane, water, carbon monoxide, hydrogen, and carbon dioxide, respectively. $h_{\mathrm{cat,o,O2}}$, and $h_{\mathrm{cat,o,N2}}$ are the specific enthalpies at the cathode exit for oxygen and nitrogen, respectively.

The energy balance also takes account the energy losses in the process ($\dot{Q}_{\mathrm{loss,sofc}}$):

$$\dot{Q}_{\mathrm{i,sofc}} = \dot{Q}_{\mathrm{o,sofc}} + \dot{Q}_{\mathrm{loss,sofc}} + \dot{W}_{\mathrm{sofc}} \quad (93)$$

HT-PEMFC

The kinetic model of the HT-PEMFC model includes the calculation of rates which account for temperature variations using Arrhenius-like expressions. These constants are used for the calculation of the anode overpotential due to CO poisoning. The CO_2, CO, CH_4, and H_2O species in the incoming syngas stream are assumed to be unreactive. The kinetic model is described in detail in (Arsalis et al., 2015).

For the calculation of the operating voltage, CO and H_2 surface coverage differentials are based on steady-state kinetic balances. The second order kinetics assumed with respect to hydrogen coverage are as follows:

$$0 = \left(k_{\mathrm{fh}} y_{\mathrm{H2}} p_{\mathrm{s}} (1 - \theta_{\mathrm{H2}} - \theta_{\mathrm{CO}})^{\mathrm{n}} - b_{\mathrm{fh}} k_{\mathrm{fh}} \theta_{\mathrm{H2}}{}^{\mathrm{n}} - i\right) \quad (94)$$

$$0 = \left(k_{\mathrm{fc}} y_{\mathrm{CO}} p_{\mathrm{s}} (1 - \theta_{\mathrm{H2}} - \theta_{\mathrm{CO}}) - b_{\mathrm{fc}} k_{\mathrm{fc}} \theta_{\mathrm{CO}} - 0.5\left(\frac{k_{\mathrm{ec}} \theta_{\mathrm{CO}}}{k_{\mathrm{eh}} \theta_{\mathrm{H2}}}\right) i\right) \quad (95)$$

θ_{CO}, and θ_{H2} are the surface coverage differentials for carbon monoxide, and hydrogen, respectively. k_{ec}, and k_{eh} are the electrooxidation rates for carbon monoxide, and hydrogen, respectively. k_{fc}, and k_{fh} are the absorption rates for carbon monoxide, and hydrogen, respectively. b_{fc}, and $b_{\mathrm{fh}}$are the desorption rates for carbon monoxide, and hydrogen, respectively.

The total activation losses are the sum of the activation losses in the anode and the cathode. They can be calculated with the Butler-Volmer equation, as follows:

$$V_{\mathrm{act,ano}} = \frac{RT_{\mathrm{s}}}{F\alpha_{\mathrm{ano}}} \operatorname{arcsinh}\left(\frac{i}{2k_{\mathrm{eh}}\theta_{\mathrm{H2}}}\right) \quad (96)$$

$$V_{\mathrm{act,cat}} = \frac{RT_{\mathrm{s}}}{4F\alpha_{\mathrm{cat}}} \ln\left(\frac{i_0 + i}{i_0}\right) \quad (97)$$

$$V_{\mathrm{act}} = V_{\mathrm{act,ano}} + V_{\mathrm{act,cat}} \quad (98)$$

α_{ano}, and α_{cat} are the symmetry factors in the anode and cathode, respectively. i_0 is the exchange current density.

The concentration losses are calculated as follows:

$$V_{\mathrm{conc}} = R_{\mathrm{diff}} \frac{i}{\lambda_{\mathrm{cat}} - 1} \quad (99)$$

R_{diff} is the cell diffusional resistance. λ_{cat} is the cathode stoichiometry.

The Ohmic losses are calculated as follows:

$$V_{\mathrm{ohm}} = iR_{\mathrm{ohm}} \quad (100)$$

R_{ohm} is the cell Ohmic resistance.

The cell voltage, the power density, the stack voltage, the stack power output, and the stack current are determined similarly to the SOFC model (see previous subsection).

The anode and cathode stoichiometries are defined as follows:

$$\lambda_{\mathrm{ano}} = \frac{\dot{n}_{\mathrm{ano,i,H2}}}{\dot{n}_{\mathrm{con,H2}}} \quad (101)$$

$$\lambda_{\mathrm{cat}} = \frac{\dot{n}_{\mathrm{cat,i,O2}}}{\dot{n}_{\mathrm{con,O2}}} \quad (102)$$

$\dot{n}_{\mathrm{ano,i,H2}}$ is the molar flow rate of hydrogen in the anode inlet, $\dot{n}_{\mathrm{con,H2}}$ is the molar flow rate of consumed hydrogen, $\dot{n}_{\mathrm{cat,i,O2}}$ is the molar flow rate of oxygen at the cathode inlet, and $\dot{n}_{\mathrm{con,O2}}$ is the molar flow rate of consumed oxygen.

The molar flow rates of consumed hydrogen, consumed oxygen, and generated water are determined as follows:

$$\dot{n}_{\mathrm{con,H2}} = I_{\mathrm{s}} \left(\frac{n_{\mathrm{cell}}}{n_{\mathrm{e}} F}\right) \quad (103)$$

$$\dot{n}_{\mathrm{con,O2}} = 0.5\dot{n}_{\mathrm{con,H2}} \quad (104)$$

$$\dot{n}_{\mathrm{gen,H2O}} = \dot{n}_{\mathrm{con,H2}} \quad (105)$$

To perform an energy balance in the HT-PEMFC stack, the mole fractions in the inlet and exits of the cathode and anode must be determined.

In the cathode inlet:

$$\dot{n}_{\mathrm{cat,i,N2}} = 3.76\dot{n}_{\mathrm{cat,i,O2}} \quad (106)$$

$$\dot{n}_{\mathrm{cat,i}} = \dot{n}_{\mathrm{cat,i,O2}} + \dot{n}_{\mathrm{cat,i,N2}} + \dot{n}_{\mathrm{cat,i,H2O}} \quad (107)$$

$$\dot{n}_{\mathrm{cat,i,H2O}} = \dot{n}_{\mathrm{cat,i}} w_{\mathrm{amb}} \quad (108)$$

$$y_{\mathrm{cat,i,O2}} = \frac{\dot{n}_{\mathrm{cat,i,O2}}}{\dot{n}_{\mathrm{cat,i}}} \quad (109)$$

$$y_{\mathrm{cat,i,N2}} = \frac{\dot{n}_{\mathrm{cat,i,N2}}}{\dot{n}_{\mathrm{cat,i}}} \quad (110)$$

$$y_{\mathrm{cat,i,H2O}} = \frac{\dot{n}_{\mathrm{cat,i,H2O}}}{\dot{n}_{\mathrm{cat,i}}} \quad (111)$$

w_{amb} is the humidity ratio.

In the cathode exit:

$$\dot{n}_{\mathrm{cat,o,O2}} = \dot{n}_{\mathrm{cat,i,O2}} - \dot{n}_{\mathrm{con,O2}} \quad (112)$$

$$\dot{n}_{\mathrm{cat,o,N2}} = \dot{n}_{\mathrm{cat,i,N2}} \quad (113)$$

$$\dot{n}_{\mathrm{cat,o,H2O}} = \dot{n}_{\mathrm{cat,i,H2O}} + \dot{n}_{\mathrm{gen,H2O}} \quad (114)$$

$$\dot{n}_{\mathrm{cat,o}} = \dot{n}_{\mathrm{cat,o,O2}} + \dot{n}_{\mathrm{cat,o,N2}} + \dot{n}_{\mathrm{cat,o,H2O}} \quad (115)$$

$$y_{\mathrm{cat,o,O2}} = \frac{\dot{n}_{\mathrm{cat,o,O2}}}{\dot{n}_{\mathrm{cat,o}}} \quad (116)$$

$$y_{\mathrm{cat,o,N2}} = \frac{\dot{n}_{\mathrm{cat,o,N2}}}{\dot{n}_{\mathrm{cat,o}}} \quad (117)$$

$$y_{\text{cat,o,H2O}} = \frac{\dot{n}_{\text{cat,o,H2O}}}{\dot{n}_{\text{cat,o}}} \tag{118}$$

In the anode inlet:

$$\dot{n}_{\text{ano,i,H2}} = y_{\text{ano,i,H2}}\dot{n}_{\text{ano,i}} \tag{119}$$

$$\dot{n}_{\text{ano,i,H2O}} = y_{\text{ano,i,H2O}}\dot{n}_{\text{ano,i}} \tag{120}$$

$$\dot{n}_{\text{ano,i,CO}} = y_{\text{ano,i,CO}}\dot{n}_{\text{ano,i}} \tag{121}$$

$$\dot{n}_{\text{ano,i,CO2}} = y_{\text{ano,i,CO2}}\dot{n}_{\text{ano,i}} \tag{122}$$

$$\dot{n}_{\text{ano,i,CH4}} = y_{\text{ano,i,CH4}}\dot{n}_{\text{ano,i}} \tag{123}$$

In the anode exit:

$$\dot{n}_{\text{ano,o,H2}} = \dot{n}_{\text{ano,i,H2}} - \dot{n}_{\text{con,H2}} \tag{124}$$

$$\dot{n}_{\text{ano,o,CO}} = \dot{n}_{\text{ano,i,CO}} \tag{125}$$

$$\dot{n}_{\text{ano,o,CO2}} = \dot{n}_{\text{ano,i,CO2}} \tag{126}$$

$$\dot{n}_{\text{ano,o,CH4}} = \dot{n}_{\text{ano,i,CH4}} \tag{127}$$

$$\dot{n}_{\text{ano,o,H2O}} = \dot{n}_{\text{ano,i,H2O}} \tag{128}$$

$$\dot{n}_{\text{ano,o}} = \dot{n}_{\text{ano,i}} - \dot{n}_{\text{con,H2}} \tag{129}$$

$$y_{\text{ano,o,H2}} = \frac{\dot{n}_{\text{ano,o,H2}}}{\dot{n}_{\text{ano,o}}} \tag{130}$$

$$y_{\text{ano,o,H2O}} = \frac{\dot{n}_{\text{ano,o,H2O}}}{\dot{n}_{\text{ano,o}}} \tag{131}$$

$$y_{\text{ano,o,CO}} = \frac{\dot{n}_{\text{ano,o,CO}}}{\dot{n}_{\text{ano,o}}} \tag{132}$$

$$y_{\text{ano,o,CO2}} = \frac{\dot{n}_{\text{ano,o,CO2}}}{\dot{n}_{\text{ano,o}}} \tag{133}$$

$$y_{\text{ano,o,CH4}} = \frac{\dot{n}_{\text{ano,o,CH4}}}{\dot{n}_{\text{ano,o}}} \tag{134}$$

Finally, an energy balance can be performed on the HT-PEMFC to determine the composition of the exhaust mixture. The energy at the inlet and the exit of the HT-PEMFC are determined as follows, respectively:

$$\begin{aligned}\dot{Q}_{\text{i,pemfc}} = {} & \dot{n}_{\text{ano,i,CH4}}h_{\text{ano,i,CH4}} + \dot{n}_{\text{ano,i,H2O}}h_{\text{ano,i,H2O}} \\ & + \dot{n}_{\text{ano,i,CO}}h_{\text{ano,i,CO}} + \dot{n}_{\text{ano,i,H2}}h_{\text{ano,i,H2}} \\ & + \dot{n}_{\text{ano,i,CO2}}h_{\text{ano,i,CO2}} + \dot{n}_{\text{cat,i,H2O}}h_{\text{cat,i,H2O}} + n_{\text{cat,i,O2}}h_{\text{cat,i,O2}} + n_{\text{cat,i,N2}}h_{\text{cat,i,N2}}\end{aligned} \tag{135}$$

$$\begin{aligned}\dot{Q}_{\text{o,pemfc}} = {} & \dot{n}_{\text{ano,o,CH4}}h_{\text{ano,o,CH4}} + \dot{n}_{\text{ano,o,H2O}}h_{\text{ano,o,H2O}} \\ & + \dot{n}_{\text{ano,o,CO}}h_{\text{ano,o,CO}} + \dot{n}_{\text{ano,o,H2}}h_{\text{ano,o,H2}} \\ & + \dot{n}_{\text{ano,o,CO2}}h_{\text{ano,o,CO2}} + \dot{n}_{\text{cat,o,H2O}}h_{\text{cat,o,H2O}} + n_{\text{cat,o,O2}}h_{\text{cat,o,O2}} + n_{\text{cat,o,N2}}h_{\text{cat,o,N2}}\end{aligned} \tag{136}$$

$h_{\text{ano,i,CH4}}$, $h_{\text{ano,i,H2O}}$, $h_{\text{ano,i,CO}}$, $h_{\text{ano,i,H2}}$, and $h_{\text{ano,i,CO2}}$ are the specific enthalpies in the anode inlet for methane, water, carbon monoxide, hydrogen, and carbon dioxide, respectively. $h_{\text{cat,i,H2O}}$, $h_{\text{cat,i,O2}}$, and $h_{\text{cat,i,N2}}$ are the specific enthalpies at the cathode inlet for water, oxygen, and nitrogen, respectively.

$h_{\text{ano,o,CH4}}$, $h_{\text{ano,o,H2O}}$, $h_{\text{ano,o,CO}}$, $h_{\text{ano,o,H2}}$, and $h_{\text{ano,o,CO2}}$ are the specific enthalpies in the anode exit for methane, water, carbon monoxide, hydrogen, and carbon dioxide, respectively. $h_{\text{cat,o,H2O}}$, $h_{\text{cat,o,O2}}$, and $h_{\text{cat,o,N2}}$ are the specific enthalpies at the cathode exit for water, oxygen, and nitrogen, respectively.

The energy balance also takes account the energy losses in the process ($\dot{Q}_{\text{loss,pemfc}}$):

$$\dot{Q}_{\text{i,pemfc}} = \dot{Q}_{\text{o,pemfc}} + \dot{Q}_{\text{loss,pemfc}} + \dot{W}_{\text{pemfc}} \tag{137}$$

Combustor

In the combustor model it is assumed that flue gas is generated in the exit of the combustor with four inlet flows, namely the PEMFC exhaust fuel mixture, the SOFC cathode exhaust air, extra air, and extra fuel. The three reactions occurring in the combustor are the following:

$$2H_2 + O_2 \rightarrow 2H_2O \tag{138}$$

$$2CO + O_2 \rightarrow 2CO_2 \tag{139}$$

$$CH_4 + 2O_2 \rightarrow CO_2 + 2H_2O \tag{140}$$

Firstly, the total molar flow rate of the needed oxygen for the combustion process must be determined. This must consider all the combustible fuels included in the mixture exiting the PEMFC stack (hydrogen, carbon monoxide, and methane) and the extra fuel (methane):

$$\dot{n}_{\text{O2,comb,stoich}} = 0.5\dot{n}_{\text{pemfc,H2}} + 0.5\dot{n}_{\text{pemfc,CO}} + 2\dot{n}_{\text{pemfc,CH4}} + 2\dot{n}_{\text{ef,CH4}} \tag{141}$$

$\dot{n}_{\text{pemfc,H2}}$, $\dot{n}_{\text{pemfc,CO}}$, and $\dot{n}_{\text{pemfc,CH4}}$ are the partial molar flow rates of hydrogen, carbon monoxide, and methane in the mixture exiting the PEMFC stack, respectively. $\dot{n}_{\text{ef,CH4}}$is the molar flow rate of the extra fuel.

The total molar flow rate of the flue gas is the sum of the partial molar flow rates of water, carbon dioxide, oxygen, and nitrogen. These can be determined as follows, respectively:

$$\dot{n}_{\text{fg,H2O}} = \dot{n}_{\text{pemfc,H2O}} + \dot{n}_{\text{pemfc,H2}} + 2\dot{n}_{\text{pemfc,CH4}} + 2\dot{n}_{\text{ef,CH4}} \tag{142}$$

$$\dot{n}_{\text{fg,CO2}} = \dot{n}_{\textit{pemfc,CO2}} + \dot{n}_{\text{pemfc,CO}} + \dot{n}_{\text{pemfc,CH4}} + \dot{n}_{\text{ef,CH4}} \tag{143}$$

$$\dot{n}_{\text{fg,O2}} = \dot{n}_{\text{pemfc,O2}} + \dot{n}_{\text{sofc,O2}} + \dot{n}_{\text{air,O2}} - \dot{n}_{\text{O2,comb,stoich}} \tag{144}$$

$$\dot{n}_{\text{fg,N2}} = \dot{n}_{\text{pemfc,N2}} + \dot{n}_{\text{sofc,N2}} + \dot{n}_{\text{air,N2}} \tag{145}$$

$$\dot{n}_{\text{fg}} = \dot{n}_{\text{fg,H2O}} + \dot{n}_{\text{fg,CO2}} + \dot{n}_{\text{fg,O2}} + \dot{n}_{\text{fg,N2}} \tag{146}$$

$\dot{n}_{\text{pemfc,H2O}}$, $\dot{n}_{\text{pemfc,O2}}$, $\dot{n}_{\text{pemfc,N2}}$, and $\dot{n}_{\textit{pemfc,CO2}}$are the partial molar flow rates of water, oxygen, nitrogen, and carbon dioxide in the mixture exiting the PEMFC stack. $\dot{n}_{\text{sofc,O2}}$, and $\dot{n}_{\text{sofc,N2}}$ are the partial molar flow rates in the mixture exiting the SOFC stack for oxygen, and nitrogen, respectively. $\dot{n}_{\text{air,O2}}$, and $\dot{n}_{\text{air,N2}}$ are the partial molar flow rates of oxygen and nitrogen in the extra air entering the combustor inlet, respectively.

The air stoichiometry can be calculated as follows:

$$\lambda_{\text{air}} = \frac{\dot{n}_{\text{pemfc,O2}} + \dot{n}_{\text{sofc,O2}} + \dot{n}_{\text{air,O2}}}{\dot{n}_{\text{O2,comb,stoich}}} \tag{147}$$

Finally, an energy balance can be performed on the combustor to determine the composition of the exhaust mixture. The energy at the inlet and the exit of the combustor are determined as follows, respectively:

$$\begin{aligned}\dot{E}_{\text{i,comb}} = {} & \dot{n}_{\text{pemfc}}\begin{pmatrix} y_{\text{pemfc,H2O}}h_{\text{pemfc,H2O}} + y_{\text{pemfc,CO2}}h_{\text{pemfc,CO2}} + y_{\text{pemfc,CO}}h_{\text{pemfc,CO}} \\ + y_{\text{pemfc,H2}}h_{\text{pemfc,H2}} + y_{\text{pemfc,CH4}}h_{\text{pemfc,CH4}} + y_{\text{pemfc,N2}}h_{\text{pemfc,N2}} \\ + y_{\text{pemfc,O2}}h_{\text{pemfc,O2}}\end{pmatrix} \\ & + \dot{n}_{\text{sofc}}\left(y_{\text{sofc,N2}}h_{\text{sofc,N2}} + y_{\text{sofc,O2}}h_{\text{sofc,O2}}\right) \\ & + \dot{n}_{\text{ef,CH4}}h_{\text{ef,CH4}} + \dot{n}_{\textit{air}}\left(y_{\text{air,N2}}h_{\text{air,N2}} + y_{\text{air,O2}}h_{\text{air,O2}}\right)\end{aligned} \tag{148}$$

$$\dot{E}_{\text{o,comb}} = \dot{n}_{\text{fg}}\left(y_{\text{fg,N2}}h_{\text{fg,N2}} + y_{\text{fg,O2}}h_{\text{fg,O2}} + y_{\text{fg,CO2}}h_{\text{fg,CO2}} + y_{\text{fg,H2O}}h_{\text{fg,H2O}}\right) \tag{149}$$

$h_{\text{pemfc,H2O}}$, $h_{\text{pemfc,CO2}}$, $h_{\text{pemfc,CO}}$, $h_{\text{pemfc,H2}}$, $h_{\text{pemfc,CH4}}$, $h_{\text{pemfc,N2}}$, and $h_{\text{pemfc,O2}}$

are the specific enthalpies in of the mixture exiting the HT-PEMFC stack for water, carbon dioxide, carbon monoxide, hydrogen, methane, nitrogen, and oxygen, respectively. $h_{\text{sofc,N2}}$, and $h_{\text{sofc,O2}}$ are the specific enthalpies of the air exiting the SOFC stack for nitrogen, and oxygen, respectively. $h_{\text{ef,CH4}}$ is the specific enthalpy of the extra fuel (methane). $h_{\text{air,N2}}$, and $h_{\text{air,O2}}$ are the specific enthalpies of the extra air for nitrogen, and oxygen, respectively. $h_{\text{fg,N2}}$, $h_{\text{fg,O2}}$, $h_{\text{fg,CO2}}$, and $h_{\text{fg,H2O}}$ are the specific enthalpies of the generated flue gas for nitrogen, oxygen, carbon dioxide, and water, respectively.

The energy balance also takes account the energy losses in the process ($\dot{Q}_{\text{loss,comb}}$):

$$\dot{E}_{\text{i,comb}} = \dot{E}_{\text{o,comb}} + \dot{Q}_{\text{loss,comb}} \tag{150}$$

Other components

The heat exchangers are modeled using the Logarithmic Mean Temperature Difference method. The water pump power input is calculated based on the volumetric flow rate of water and pressure difference (boost) between inlet and outlet. For the purpose of brevity, these are not provided in detail.

Total system

The net electrical power output of the hybrid SOFC—HT-PEMFC system is defined as follows:

$$\dot{W}_{\text{el,net}} = \dot{W}_{\text{sofc}} + \dot{W}_{\text{pemfc}} - \dot{W}_{\text{pump}} \tag{151}$$

$\dot{W}_{\text{pump}}$ is the electrical power input to the water pump.

The net electrical efficiency of the hybrid system is determined on a Lower Heating Value (LHV) basis. This efficiency is the ratio of the net power output generated by the hybrid system ($\dot{W}_{\text{el,net}}$) to the chemical energy of methane fuel supplied to the system ($\dot{E}_{\text{fuel,LHV}}$), as follows:

$$\eta_{\text{el,net,LHV}} = \frac{\dot{W}_{\text{el,net}}}{\dot{E}_{\text{fuel,LHV}}} \tag{152}$$

where $\dot{E}_{\text{fuel,LHV}}$ is the rate of chemical energy of the supplied fuel to the system, and can be calculated as follows:

$$\dot{E}_{\text{fuel,LHV}} = \dot{n}_1 LHV_{\text{CH4}} \tag{153}$$

LHV_{CH4} is the lower heating value of methane and is equal to 802.5 MJ/kmol.

System optimization

The optimum performance of the proposed hybrid system is achieved when its net electrical efficiency is maximized. The built-in min/max capability of EES (Klein, 2022) is used to reach this optimum value, while selected independent variables are allowed to vary. The procedure follows the system optimization previously published by the author in (Arsalis et al., 2013). The mathematical formulation of the optimization problem can be expressed as the maximization of the net electrical efficiency subject to both equality $\vec{h}(\vec{x}, \vec{y})$, and inequality $\vec{g}(\vec{x}, \vec{y})$ constraints:

Table 2
Parameters remaining fixed during the optimization process.

Variable	Description	Value
$A_{\text{s,pemfc}}$	Active area of PEMFC	45.16 cm^2
$A_{\text{s,sofc}}$	Active area of SOFC	100 cm^2
$\dot{W}_{\text{el,net}}$	Net electrical power output of the hybrid system	6 kW

Table 3
Initial, minimum, maximum, and optimum values of the independent variables for the optimization process.

Variable	Description (unit)	Initial	Min	Max	Optimum
λ_{ano}	HT-PEMFC anode stoichiometry [-]	1.35	1.15	1.55	1.41
SC	Steam-to-carbon ratio [-]	2.75	2.50	3.00	2.50
T_{14}	Flue gas temperature at combustor exit [K]	1003	983	1023	983
U_{f}	SOFC fuel utilization [-]	0.90	0.88	0.92	0.92

$$\max f(\vec{x}, \vec{y}) \text{ subjected to } \begin{matrix} \vec{h}(\vec{x}, \vec{y}) = 0 \\ \vec{g}(\vec{x}, \vec{y}) \leq 0 \end{matrix} \tag{154}$$

The parameters remaining fixed during the optimization process are given in Table 2. All available independent variables are included in the optimization process, namely: anode stoichiometry (λ_{ano}), steam-to-carbon ratio (SC), flue gas temperature at the exit of the combustor (T_{14}), and fuel utilization(U_{f}). Table 3 includes their initial, minimum, and maximum values, as applied in the optimization process. The minimum and maximum values of the independent variables derive from the restrictions on the simulation model, which are set in such a way that only allows simulation within a realistic operational range.

Cost model

In addition to the technical analysis of the hybrid system, a cost model is developed to assess the economic performance of the proposed hybrid system. This also facilitates an economic comparison with the standalone HT-PEMFC and SOFC systems. The cost model assumes that the fuel is natural gas, and the currency unit is USD ($). For simplicity it

Table 4
Cost model for the hybrid SOFC—HT-PEMFC system.

Cost parameter	Description (unit)
$c_{\text{fy}} = E_{\text{py}} c_{\text{fuel}}$	Annual cost of fuel [$/year]
$C_{\text{sys}} = c_{\text{sofc}}\dot{W}_{\text{sofc}} + c_{\text{pemfc}}\dot{W}_{\text{pemfc}} + (c_{\text{smr}} + c_{\text{wgs}} + c_{\text{comb}} + c_{\text{hex}} + c_{\text{des}} + c_{\text{pump}} + c_{\text{aux}})\dot{W}_{\text{el,net}}$	Total cost of system [$]
$C_{\text{down}} = (1 - f_{\text{loan}})C_{\text{sys}}$	Down payment [$]
$AP_1 = \frac{r_1}{1-(1+r_1)^{-N_{\text{lt}}}}, r_1 = r_{\text{mL}} - i$	Capital recovery factors [-]
$AP_2 = \frac{r_2}{1-(1+r_2)^{-N_{\text{lt}}}}, r_2 = r_{\text{mL}}$	
$AP_3 = \frac{r_3}{1-(1+r_3)^{-N_{\text{lt}}}}, r_3 = \frac{r_2 - r_1}{0.01 + r_1}$	
$AP_4 = \frac{r_4}{1-(1+r_4)^{-N_{\text{lt}}}}, r_4 = \frac{r_{\text{mL}} - r_{\text{e}}}{1 + r_{\text{e}}}$	
$C_{\text{loan}} = \left(\frac{AP_1}{AP_2}\right) f_{\text{loan}} C_{\text{sys}}$	Cost of the loan [$]
$D_{\text{loan}} = t\left(\frac{AP_1}{AP_2} - \frac{AP_1 - r_1}{(1+r_1)AP_3}\right) f_{\text{loan}} C_{\text{sys}}$	Tax deduction on the loan [$]
$C_{\text{twc}} = C_{\text{down}} + C_{\text{loan}} - D_{\text{loan}}$	Total worth of capital [$]
$PA_2 = \frac{1}{AP_2}$	Uniform series present worth factor [-]
$D_{\text{dep}} = tPA_2\left(\frac{C_{\text{sys}}}{N_{\text{lt}}}\right)$	Depreciation of capital [$]
$D_{\text{cred}} = t_{\text{cred}} C_{\text{sys}}$	Tax credit [$]
$FP_2 = (1 + r_2)^{-N_{\text{lt}}}$	Compound amount factor [-]
$PF_2 = \frac{1}{FP_2}$	Present worth factor [-]
$D_{\text{salv}} = f_{\text{salv}} C_{\text{sys}} PF_2 (1 - t_{\text{salv}})$	Salvage worth [$]
$C_{\text{prop}} = f_{\text{prop}} C_{\text{sys}} t_{\text{prop}} (1 - t)$	Tax paid on property [$]
$C_{\text{omi}} = f_{\text{omi}} C_{\text{sys}} (PA_2)(1 - t)$	Cost of operation, maintenance, and insurance [$]
$C_{\text{tcf}} = c_{\text{fy}}\left(\frac{1-t}{AP_4}\right)$	Total cost of fuel [$]
$LCC = C_{\text{twc}} + C_{\text{prop}} + C_{\text{omi}} + C_{\text{tcf}} - (D_{\text{dep}} + D_{\text{cred}} + D_{\text{salv}})$	Lifecycle cost [$]

Table 5
Constant cost parameters for the proposed hybrid SOFC—HT-PEMFC system.

Cost parameter	Description	Value	Ref.
c_{fuel}	Cost of fuel in the first year	3.771E-8 $/J	(ycharts.com, 2022)
c_{sofc}	Specific cost of SOFC stack	2 $/W	(Whiston et al., 2021)
c_{pemfc}	Specific cost of HT-PEMFC stack	1.23 $/W	(Lange and Poulsen, 2016)
c_{smr}	Specific cost of SMR reactor	0.18 $/W	(Ogden, 2001)
c_{wgs}	Specific cost of WGS reactor	0.13 $/W	(Nexant Inc., 2006)
c_{comb}	Specific cost of combustor	0.05 $/W	(IEA, 2015)
c_{hex}	Specific cost of heat exchangers	0.25 $/W	(Lalanne and Byrne, 2019)
c_{des}	Specific cost of desulfurizer	0.033 $/W	(Nexant Inc., 2006)
c_{pump}	Specific cost of water pump	0.02 $/W	(Nexant Inc., 2006)
c_{aux}	Specific cost of water separator, water tank, and valves	0.05 $/W	(IEA, 2015)
N_{lt}	System lifetime	5 years	(Scataglini et al., 2015)
r_e	Real fuel price escalation rate	0.1	(Dincer and Zamfirescu, 2011)
i	Inflation rate	0.01	(Dincer and Zamfirescu, 2011)
r_m	Market discount rate	0.06	(Dincer and Zamfirescu, 2011)
r_{mL}	Market loan rate	0.05	(Dincer and Zamfirescu, 2011)
f_{loan}	Fraction of the capital cost that is paid through a loan	0.8	(Dincer and Zamfirescu, 2011)
t	Incremental income tax	0.4	(Dincer and Zamfirescu, 2011)
t_{cred}	Tax credit	0.02	(Dincer and Zamfirescu, 2011)
f_{salv}	Salvage factor	0.1	(Dincer and Zamfirescu, 2011)
t_{salv}	Tax perceived by the government when the salvage is valorized	0.2	(Dincer and Zamfirescu, 2011)
f_{prop}	Property factor	0.5	(Dincer and Zamfirescu, 2011)
t_{prop}	Tax on the property	0.25	(Dincer and Zamfirescu, 2011)
f_{omi}	Operation, maintenance, and insurance factor	0.01	(Dincer and Zamfirescu, 2011)

is also assumed that the performance of the components does not deteriorate over time, and that the lifetime of all components is 5 years with continuous operation (i.e., 8760 h per year) at full load. The model is adapted for the purposes of the current study from the analysis found in (Dincer and Zamfirescu, 2011). The cost model equations for the hybrid SOFC—HT-PEMFC system are given in Table 4, while the values of the constant cost parameters are given in Table 5.

Results and discussion

This section starts with a validation of the SOFC and HT-PEMFC subsystem models with available experimental data. Next, the results deriving from the application of the optimization methodology on the proposed hybrid system are presented and discussed in detail. A case study is then conducted to show the feasibility of the proposed system when used for real cases. This is done through comparison with equivalent, standalone HT-PEMFC and SOFC systems. Apart from the technical behavior of the proposed system, a cost analysis is conducted to compare the economic performance of the proposed hybrid system with the standalone HT-PEMFC and SOFC systems.

Model validation

The system model cannot be validated as a whole, because due to the novelty of the system design, similar, comparable systems are not available in the open literature. However, the fuel cell models can be validated with available experimental data. These validations are already available in some previous publications of the author. Specifically, the SOFC stack model was validated in (Arsalis and Georghiou, 2019), while the HT-PEMFC stack model was validated in (Arsalis et al., 2012).

Application of the optimization process

The purpose of applying the optimization process (described in sub Section 3.8) to the proposed hybrid system is to maximize its net electrical efficiency. The net electrical efficiency of the pre-optimized system is 0.4225. This value is obtained with the constant parameter values and the initial values of the independent variables shown in Table 3. The optimum value of the objective function is found following the optimization process described in detail in (Arsalis et al., 2012). The final optimized value, which is found at the 128th generation, is 0.4360. The evolution of the objective function throughout the optimization process is shown graphically in Fig. 4. The maximization of the objective function is marginal (1.35 %) due to the largely complex system configuration, which does not allow a lot of room for variation for the independent variables within an acceptable level in terms of allowable system functionality. The optimum values of the independent variables are given in Table 3 (see rightmost column). As it can be seen from the results, the optimum values for the steam-to-carbon ratio and the flue gas temperature at the combustor exit are the minimum values set in the optimization process, while the optimum value for the utilization factor is the maximum one.

Case study: operational performance of the proposed hybrid SOFC—HT-PEMFC system at design conditions and comparison with standalone HT-PEMFC and SOFC systems

A case study is conducted to identify the feasibility of the proposed hybrid SOFC—HT-PEMFC system when operated at design conditions. Values of key thermophysical properties (molar flow rate, pressure, temperature, and mole fractions) for every state (node) shown in Fig. 1 for the optimum system configuration are given in Table 6. In terms of contribution to the net electrical power output of the total system, the SOFC subsystem provides 5681 W, while the HT-PEMFC subsystem provides an additional 319 W. This means that the optimization process has favored a much larger SOFC subsystem in comparison to the HT-PEMFC subsystem due to the fact that the former performs at a much higher efficiency than the latter. This is also the reason why the utilization factor of the SOFC subsystem has moved towards the maximum value allowed by the variation process.

It is also important to compare the technical characteristics and resulting performance of the proposed hybrid SOFC—HT-PEMFC system with the standalone HT-PEMFC and SOFC based systems described in detail in Section 2. All three systems are assumed to be operating with the same parameters and conditions and generate the exact same electrical power output (6 kWe). Also, the standalone HT-PEMFC and SOFC based systems have been optimized in a similar way as for the case of the proposed hybrid SOFC—HT-PEMFC system (following the procedure described in sub Section 3.8). The key parameters that are selected for this comparison are the net electrical efficiency, the annual fuel (CH_4) consumption, and the annual generation of CO_2 emissions; the values for

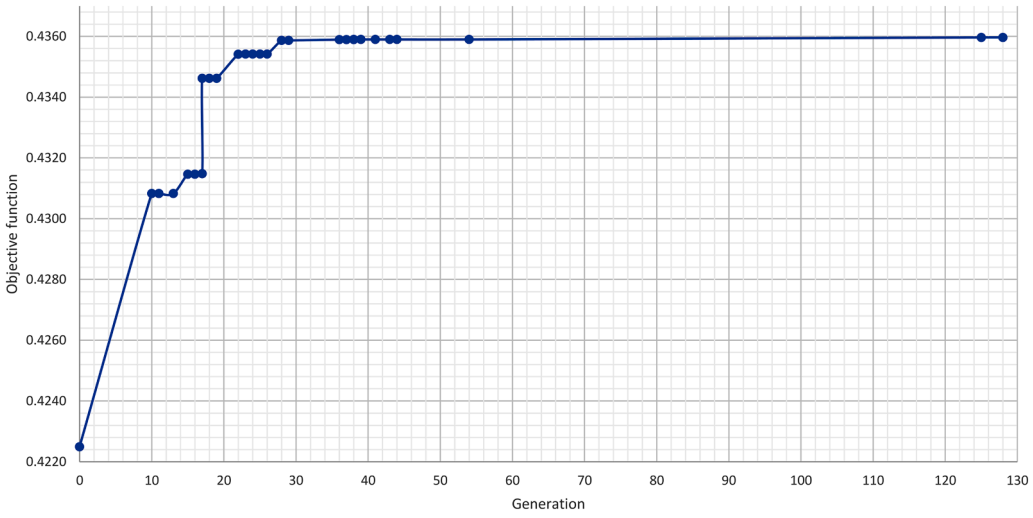

Fig. 4. Evolution of the objective function throughout the optimization process.

Table 6
Values of the thermophysical properties for the proposed hybrid SOFC—HT-PEMFC system when operated at design conditions.

Node	n_i [kmol/s]	p_i [Pa]	T_i [K]	$y_{CH_4,i}$	$y_{CO,i}$	$y_{CO_2,i}$	$y_{H_2,i}$	$y_{H_2O,i}$	$y_{N_2,i}$	$y_{O_2,i}$
1	0.000017	120,000	288	1.000	0.000	0.000	0.000	0.000	0.000	0.000
2	0.000012	120,000	288	1.000	0.000	0.000	0.000	0.000	0.000	0.000
3	0.000012	119,000	288	1.000	0.000	0.000	0.000	0.000	0.000	0.000
4	0.000012	118,000	723	1.000	0.000	0.000	0.000	0.000	0.000	0.000
5	0.000060	118,000	723	0.286	0.000	0.000	0.000	0.714	0.000	0.000
6	0.000060	117,000	933	0.031	0.088	0.075	0.561	0.246	0.000	0.000
7	0.000064	116,000	983	0.000	0.009	0.173	0.058	0.761	0.000	0.000
8	0.000064	115,000	523	0.000	0.009	0.173	0.058	0.761	0.000	0.000
9	0.000064	114,000	536	0.000	0.000	0.174	0.079	0.747	0.000	0.000
10	0.000064	113,000	433	0.000	0.000	0.174	0.079	0.747	0.000	0.000
11	0.000325	112,000	431	0.000	0.000	0.034	0.005	0.168	0.631	0.162
12	0.000325	111,000	455	0.000	0.000	0.034	0.005	0.168	0.631	0.162
13	0.000325	110,000	568	0.000	0.000	0.034	0.005	0.168	0.631	0.162
14	0.002374	115,000	983	0.000	0.000	0.007	0.000	0.028	0.774	0.191
15	0.002374	114,000	951	0.000	0.000	0.007	0.000	0.028	0.774	0.191
16	0.000149	112,000	748	0.000	0.000	0.007	0.000	0.028	0.774	0.191
17	0.000149	111,000	374	0.000	0.000	0.007	0.000	0.028	0.774	0.191
18	0.002225	113,000	374	0.000	0.000	0.007	0.000	0.028	0.774	0.191
19	0.000029	100,000	298	0.000	0.000	0.000	0.000	1.000	0.000	0.000
20	0.000029	119,000	298	0.000	0.000	0.000	0.000	1.000	0.000	0.000
21	0.000029	118,000	723	0.000	0.000	0.000	0.000	1.000	0.000	0.000
22	0.002065	101,325	298	0.000	0.000	0.000	0.000	0.000	0.790	0.210
23	0.002065	100,325	933	0.000	0.000	0.000	0.000	0.000	0.790	0.210
24	0.002044	116,000	983	0.000	0.000	0.000	0.000	0.000	0.798	0.202
25	0.000264	101,325	298	0.000	0.000	0.000	0.000	0.000	0.790	0.210
26	0.000006	120,000	288	1.000	0.000	0.000	0.000	0.000	0.000	0.000
27	0.000000	101,325	298	0.000	0.000	0.000	0.000	0.000	0.790	0.210
28	0.002225	114,000	951	0.000	0.000	0.007	0.000	0.028	0.774	0.191
29	0.000149	114,000	951	0.000	0.000	0.007	0.000	0.028	0.774	0.191
30	0.000149	113,000	798	0.000	0.000	0.007	0.000	0.028	0.774	0.191
31	0.000325	109,000	640	0.000	0.000	0.034	0.005	0.168	0.631	0.162

these parameters are shown in Fig. 5, Fig. 6, and Fig. 7, respectively. As shown from the results, the proposed hybrid SOFC—HT-PEMFC system outperforms both the HT-PEMFC and the SOFC systems. It is also important to note that these three key parameters are interrelated, since the higher net electrical efficiency achieved by the proposed system allows a reduction of both fuel consumption and CO_2 emissions.

Another important criterion for the feasibility of the proposed system is its economic performance. Through the developed cost model (see sub Section 3.9), the proposed system is compared with the standalone HT-PEMFC and SOFC systems. The most significant economic factors are the total capital (initial) system cost, the total cost of fuel (for the whole system lifetime; assuming continuous operation at design conditions), and the lifecycle cost (LCC). The results of the economic analysis are shown in Table 7. The proposed system has a higher capital cost than the two standalone systems, because a higher number of components have been integrated for its formation, in comparison to the standalone systems. However, the total cost of fuel for the proposed hybrid system is significantly lower. This is due to the fact that the higher net electrical efficiency achieved in the proposed system reduces fuel consumption. Overall, the LCC, which is the most significant economic parameter, is lower for the proposed system, which clearly suggests that the proposed system is more economically competitive than both standalone systems. This is because the LCC is mostly dependent on the total cost of fuel. The specific savings generated from the proposed system in comparison to the HT-PEMFC and SOFC systems are 42.7 % and 5.6 %, respectively. Finally, the unit cost of electricity is estimated at $0.244 per kWh, based

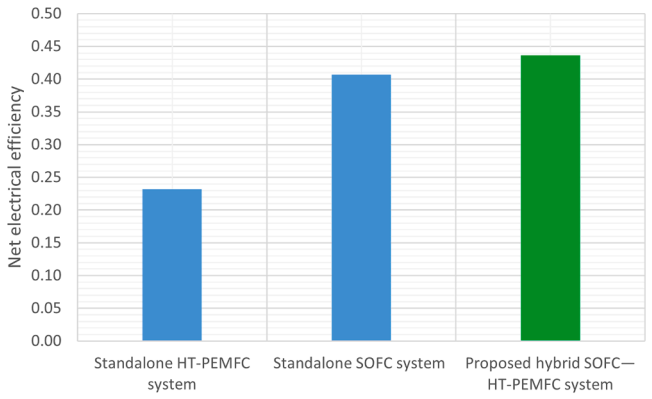

Fig. 5. Performance comparison of the proposed hybrid SOFC—HT-PEMFC system with the standalone HT-PEMFC and SOFC based systems in terms of net electrical efficiency.

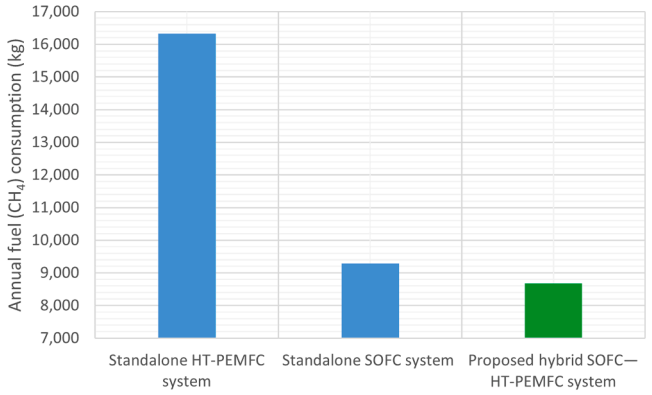

Fig. 6. Performance comparison of the proposed hybrid SOFC—HT-PEMFC system with the standalone HT-PEMFC and SOFC based systems in terms of annual fuel (CH_4) consumption.

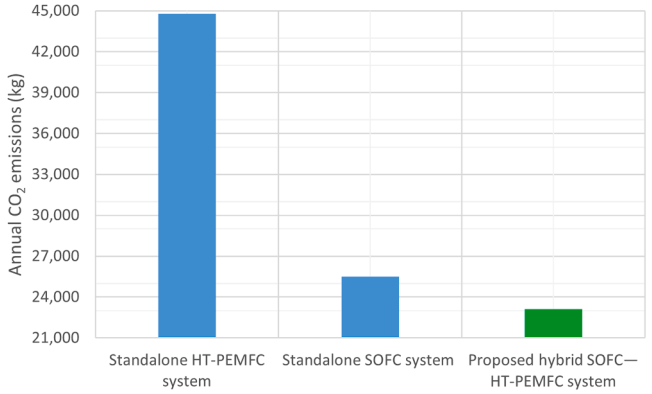

Fig. 7. Performance comparison of the proposed hybrid SOFC—HT-PEMFC system with the standalone HT-PEMFC and SOFC based systems in terms of annual CO_2 emissions.

on the definition provided in (Arsalis and Georghiou, 2018).

Conclusions

This study presents a detailed design, modeling, and optimization of a novel natural gas fueled, 6 kWe hybrid SOFC—HT-PEMFC system. An innovative design is proposed and adopted, combining SOFC and HT-PEMFC technologies in an integrated total energy system.

Table 7
Cost analysis of the proposed hybrid SOFC—HT-PEMFC system and comparison with the standalone HT-PEMFC and SOFC based systems.

Parameter	Standalone HT-PEMFC system	Standalone SOFC system	Proposed hybrid SOFC—HT-PEMFC system
Total cost of system [$]	11,658	15,498	16,032
Total cost of fuel [$]	106,472	60,595	56,574
Lifecycle cost [$]	111,942	67,867	64,097

Additionally, the proposed design makes optimum use of thermal management, in an effort to maximize the net electrical efficiency of the system, within a practical and realistic configuration. Moreover, the study investigates the possible advantages of such a system, in both technical and economic aspects. In terms of modeling limitations, a zero-dimensional, steady state model has been adopted, which neglects the dynamic behavior of system components. After modeling each component/subsystem, the total system model is optimized with the objective function aiming to maximize the net electrical efficiency of the hybrid system. The system is optimized with a genetic algorithm-based optimization strategy, reaching a net electrical efficiency of 43.6 %. The proposed hybrid system outperforms equivalent (same net electrical power output), standalone HT-PEMFC and SOFC systems, which perform at net electrical efficiencies of 23.2 % and 40.7 %, respectively.

A cost analysis is also conducted to investigate the economic performance of the proposed hybrid system and compare it to the HT-PEMFC and SOFC systems. Although the proposed system has a higher capital cost than both of the aforementioned systems, due to the increased number of components that comprise it, it has a lower total cost of fuel due to its superior efficiency, which allows a reduction of the required natural gas consumption. For the LCC, the total cost of fuel is significantly more influential than the total cost of the system, and therefore the proposed hybrid system outperforms both the HT-PEMFC and SOFC standalone systems, achieving the lowest LCC. Specifically, the LCC for the proposed system is $64,097. In comparison with the standalone HT-PEMFC and SOFC systems, the proposed system achieves savings of 42.7 % and 5.6 %, respectively, in comparison to the standalone HT-PEMFC and SOFC systems. The estimated unit cost of electricity for the proposed system is $0.244 per kWh, which suggests that it could be competitive in regions with currently higher costs of electricity. The proposed system benefited from the current high cost of natural gas, which has risen enormously in the last year (2022). The proposed hybrid system is also a cleaner option in terms of CO_2 gas emissions, since it generates 23,100 kg-CO_2 per year in comparison to 44,794 and 25,494 kg for the HT-PEMFC system, and the SOFC system, respectively. Therefore, with the current high rising costs for natural gas and the need for reduction of carbon emissions, such highly efficient systems are likely to become key options for the future energy infrastructure.

CRediT authorship contribution statement

Alexandros Arsalis: Writing – review & editing, Writing – original draft, Visualization, Validation, Supervision, Software, Resources, Project administration, Methodology, Investigation, Formal analysis, Data curation.

Declaration of competing interest

The authors declare that they have no known competing financial interests or personal relationships that could have appeared to influence the work reported in this paper.

Data availability

Data will be made available on request.

Funding

This research did not receive any specific grant from funding agencies in the public, commercial, or not-for-profit sectors.

References

Arsalis, A., 2019. A comprehensive review of fuel cell-based micro-combined-heat-and-power systems. Renew. Sustain. Energy Rev. 105, 391–414. https://doi.org/10.1016/j.rser.2019.02.013.

Arsalis, A., 2008. Thermoeconomic modeling and parametric study of hybrid SOFC-gas turbine-steam turbine power plants ranging from 1.5 to 10 MWe. J. Power Sources 181, 313–326. https://doi.org/10.1016/j.jpowsour.2007.11.104.

Arsalis, A., Georghiou, G.E., 2019. Thermoeconomic optimization of a hybrid photovoltaic-solid oxide fuel cell system for decentralized application. Appl. Sci. 9, 5450. https://doi.org/10.3390/app9245450.

Arsalis, A., Georghiou, G.E., 2018. A decentralized, hybrid photovoltaic-solid oxide fuel cell system for application to a commercial building. Energies 11, 3512. https://doi.org/10.3390/en11123512.

Arsalis, A., Kær, S.K., Nielsen, M.P., 2015. Modeling and optimization of a heat-pump-assisted high temperature proton exchange membrane fuel cell micro-combined-heat-and-power system for residential applications. Appl. Energy 147, 569–581. https://doi.org/10.1016/j.apenergy.2015.03.031.

Arsalis, A., Nielsen, M.P., Kær, S.K., 2013. Optimization of a high temperature PEMFC micro-CHP system by formulation and application of a process integration methodology. Fuel Cells 13, 238–248. https://doi.org/10.1002/fuce.201200102.

Arsalis, A., Nielsen, M.P., Kær, S.K., 2012. Modeling and optimization of a 1 kWe HT-PEMFC-based micro-CHP residential system. Int. J. Hydrogen Energy 37, 2470–2481. https://doi.org/10.1016/j.ijhydene.2011.10.081.

Arsalis, A., Nielsen, M.P., Kær, S.K., 2011. Modeling and off-design performance of a 1 kWe HT-PEMFC (high temperature-proton exchange membrane fuel cell)-based residential micro-CHP (combined-heat-and-power) system for Danish single-family households. Energy 36, 993–1002. https://doi.org/10.1016/j.energy.2010.12.009.

Barbir, F., 2013. Pem Fuel cells: Theory and Practice, 2nd ed. Elsevier Academic Press, Burlington, MA, USA.

Büchi, F.N., Inaba, M., Schmidt, T.J., 2009. Polymer Electrolyte Fuel Cell Durability. Springer, New York, NY, USA. https://doi.org/10.1007/978-0-387-85536-3.

Calise, F., Dentice d' Accadia, M., Vanoli, L., von Spakovsky, M.R., 2007. Full load synthesis/design optimization of a hybrid SOFC-GT power plant. Energy 32, 446–458. https://doi.org/10.1016/j.energy.2006.06.016.

Calise, F., Dentice d' Accadia, M., Vanoli, L., von Spakovsky, M.R., 2006a. Single-level optimization of a hybrid SOFC-GT power plant. J. Power Sources 159, 1169–1185. https://doi.org/10.1016/j.jpowsour.2005.11.108.

Calise, F., Dentice d'Accadia, M., Libertini, L., Quiriti, E., Vanoli, R., Vicidomini, M., 2017. Optimal operating strategies of combined cooling, heating and power systems: a case study for an engine manufacturing facility. Energy Convers. Manag. 149, 1066–1084. https://doi.org/10.1016/j.enconman.2017.06.028.

Calise, F., Dentice d'Accadia, M., Palombo, A., Vanoli, L., 2006b. Simulation and exergy analysis of a hybrid solid oxide fuel cell (SOFC)-Gas turbine system. Energy 31, 3278–3299. https://doi.org/10.1016/j.energy.2006.03.006.

Davies, J., Lihou, D., 1971. Optimal design of methane steam reformer. Chem. Proc. Eng. 52, 71–80.

Dicks, A.L., Fellows, R.G., Martin Mescal, C., Seymour, C., 2000. A study of SOFC–PEM hybrid systems. J. Power Sources 86, 501–506. https://doi.org/10.1016/S0378-7753(99)00492-9.

Dincer, I., Zamfirescu, C., 2011. Sustainable Energy Systems and Applications. Springer, New York, NY.

Hubert, C.E., Achard, P., Metkemeijer, R., 2006. Study of a small heat and power PEM fuel cell system generator. J. Power Sources 156, 64–70. https://doi.org/10.1016/j.jpowsour.2005.08.022.

IEA, 2015. Technology roadmap - hydrogen and fuel cells, https://www.iea.org/reports/technology-roadmap-hydrogen-and-fuel-cells. Paris, IEA License: CC BY 4.0.

Jaluria, Y., 2008. Design and Optimization of Thermal Systems, 2nd ed. CRC Press, Boca Raton, FL.

Keiski, R.L., Salmi, T., Niemisto, P., Ainassaari, J., Pohjola, V.J., 1996. Stationary and transient kinetics of the high temperature water-gas shift reaction. Appl. Catal. A Gen. 137, 349–370. https://doi.org/10.1016/0926-860X(95)00315-0.

Kim, H.R., Seo, M.H., Ahn, J.H., Kim, T.S., 2023. Thermodynamic design and analysis of SOFC/PEMFC hybrid systems with cascade effects: a perspective on complete carbon dioxide capture and high efficiency. Energy Rep. 9, 2335–2347. https://doi.org/10.1016/j.egyr.2023.01.048.

Kim, K., Von Spakovsky, M.R., Wang, M., Nelson, D.J., 2011. A hybrid multi-level optimization approach for the dynamic synthesis/design and operation/control under uncertainty of a fuel cell system. Energy 36, 3933–3943. https://doi.org/10.1016/j.energy.2010.08.024.

Klein, S.A., 2022. EES – Engineering Equation Solver, Version 11.317, April 5, 2023 F-Chart Software, https://fchartsoftware.com.

Lalanne, P., Byrne, P., 2019. Large-scale pumped thermal electricity storages-converting energy using shallow lined rock caverns, carbon dioxide and underground pumped-hydro. Appl. Sci. 9 https://doi.org/10.3390/app9194150.

Lange, C.J., Poulsen, J.A., 2016. Valuing Learning Effects As a Real Option: Application to PEM Fuel Cells in the Indian Telcomarket. Copenhagen Business School.

Larminie, J., Dicks, A.L., 2003. Fuel Cell Systems Explained, 2nd ed. Wiley, Chichester, UK.

Li, L., Vellayani Aravind, P., Woudstra, T., van den Broek, M., 2023. Assessing the waste heat recovery potential of liquid organic hydrogen carrier chains. Energy Convers. Manag. 276 https://doi.org/10.1016/j.enconman.2022.116555.

Meng, T., Cui, D., Ji, Y., Cheng, M., Tu, B., Lan, Z., 2022. Optimization and efficiency analysis of methanol SOFC-PEMFC hybrid system. Int. J. Hydrogen Energy 47, 27690–27702. https://doi.org/10.1016/j.ijhydene.2022.06.102.

Milewski, J., Szczęśniak, A., Szabłowski, Ł., 2021. A proton conducting solid oxide fuel cell—Implementation of the reduced order model in available software and verification based on experimental data. J. Power Sources 502. https://doi.org/10.1016/j.jpowsour.2021.229948.

Napoli, R., Gandiglio, M., Lanzini, A., Santarelli, M., 2015. Techno-economic analysis of PEMFC and SOFC micro-CHP fuel cell systems for the residential sector. Energy Build 103, 131–146. https://doi.org/10.1016/j.enbuild.2015.06.052.

Nexant Inc., 2006. *Equipment Design and Cost Estimation for Small Modular Biomass Systems, Synthesis Gas Cleanup, and Oxygen Separation Equipment; Task 1: Cost Estimates of Small Modular Systems*. Golden, Colorado, USA. https://doi.org/10.2172/882499.

O'Hayre, R., Colella, W., Cha, S.W., Prinz, F.B., 2009. Fuel Cell Fundamentals, 2nd ed. Wiley, Hoboken, New Jersey.

Ogden, J.M., 2001. Review of small stationary reformers for hydrogen production. Environ. Stud. 63.

Pourrahmani, H., Gay, M., Van herle, J., 2021. Electric vehicle charging station using fuel cell technology: two different scenarios and thermodynamic analysis. Energy Rep. 7, 6955–6972. https://doi.org/10.1016/j.egyr.2021.09.211.

Rangel-Hernández, V.H., Fang, Q., Blum, L., Ramírez-Minguela, J.J., Zaleta-Aguilar, A., 2020. Impact of operational and design variables on the thermodynamic behavior of a simulated 500 kw ng-fueled solid oxide fuel cell stack. Energy Convers. Manag. 204 https://doi.org/10.1016/j.enconman.2019.112283.

Rosli, R.E., Sulong, A.B., W. Daud, W.R., Zulkifley, M.A., Rosli, M.I., Majlan, E.H., Haque, M.A., M. Radzuan, N.A., 2019. The design and development of an HT-PEMFC test cell and test station. Int. J. Hydrogen Energy 44, 30763–30771. https://doi.org/10.1016/j.ijhydene.2018.01.174.

Scataglini, R., Mayyas, A., Wei, M., Chan, S.H., Lipman, T., Gosselin, D., D'Alessio, A., Breunig, H., Colella, W.G., James, B.D., 2015. *A Total Cost of Ownership Model For Solid Oxide Fuel Cells in Combined Heat and Power and Power-Only Applications*. Berkeley, CA.

Siegel, C., Bandlamudi, G., Filusch, F., Heinzel, A., 2011. Locally resolved measurements in a segmented HTPEM fuel cell with straight flow-fields. Fuel Cells 11, 489–500. https://doi.org/10.1002/fuce.201000101.

Stolten, D., 2010. Hydrogen and Fuel Cells: Fundamentals, Technologies and Applications, 1st ed. Wiley-VCH, Weinheim, Germany.

Subramanyan, K., Diwekar, U.M., Goyal, A., 2004. Multi-objective optimization for hybrid fuel cells power system under uncertainty. J. Power Sources 132, 99–112. https://doi.org/10.1016/j.jpowsour.2003.12.053.

Tan, L., Yang, C., Zhou, N., 2015. Synthesis/design optimization of SOFC–PEM hybrid system under uncertainty. Chinese J. Chem. Eng. 23, 128–137. https://doi.org/10.1016/j.cjche.2014.09.040.

Wahl, S., Gallet, A., Horstmann, P., Carr, M., Bessler, W.G., Lapicque, F., Friedrich, K.A., 2015. Modeling of a thermally integrated 10kW e planar solid oxide fuel cell system with anode offgas recycling and internal reforming by discretization in fl ow direction 279, 656–666.

Whiston, M.M., Lima Azevedo, I.M., Litster, S., Samaras, C., Whitefoot, K.S., Whitacre, J. F., 2021. Paths to market for stationary solid oxide fuel cells: expert elicitation and a cost of electricity model. Appl. Energy 304. https://doi.org/10.1016/j.apenergy.2021.117641.

Wu, Z., Tan, P., Chen, B., Cai, W., Chen, M., Xu, X., Zhang, Z., Ni, M., 2019. Dynamic modeling and operation strategy of an NG-fueled SOFC-WGS-TSA-PEMFC hybrid energy conversion system for fuel cell vehicle by using MATLAB/SIMULINK. Energy 175, 567–579. https://doi.org/10.1016/j.energy.2019.03.119.

Wu, Z., Yao, J., Zhu, P., Yang, F., Meng, X., Kurko, S., Zhang, Z., 2021a. Study of MW-scale biogas-fed SOFC-WGS-TSA-PEMFC hybrid power technology as distributed energy system: thermodynamic, exergetic and thermo-economic evaluation. Int. J. Hydrogen Energy 46, 11183–11198. https://doi.org/10.1016/j.ijhydene.2020.02.111.

Wu, Z., Zhang, Z., Ni, M., 2018. Modeling of a novel SOFC-PEMFC hybrid system coupled with thermal swing adsorption for H2 purification: parametric and exergy analyses. Energy Convers. Manag. 174, 802–813. https://doi.org/10.1016/j.enconman.2018.08.073.

Wu, Z., Zhu, P., Yao, J., Kurko, S., Ren, J., Tan, P., Xu, H., Zhang, Z., Ni, M., 2021b. Methanol to power through high-efficiency hybrid fuel cell system: thermodynamic, thermo-economic, and techno-economic (3T) analyses in Northwest China. Energy Convers. Manag. 232 https://doi.org/10.1016/j.enconman.2021.113899.

Wu, Z., Zhu, P., Yao, J., Tan, P., Xu, H., Chen, B., Yang, F., Zhang, Z., Ni, M., 2020. Thermo-economic modeling and analysis of an NG-fueled SOFC-WGS-TSA-PEMFC hybrid energy conversion system for stationary electricity power generation. Energy 192. https://doi.org/10.1016/j.energy.2019.116613.

Yan, H., Wang, G., Lu, Z., Tan, P., Kwan, T.H., Xu, H., Chen, B., Ni, M., Wu, Z., 2020. Techno-economic evaluation and technology roadmap of the MWe-scale SOFC-

PEMFC hybrid fuel cell system for clean power generation. J. Clean. Prod. 255 https://doi.org/10.1016/j.jclepro.2020.120225.
ycharts.com, 2022. European Union Natural Gas Import Price [WWW Document]. URL https://ycharts.com/indicators/europe_natural_gas_price (accessed 12.7.22).
Zhao, Y., Sadhukhan, J., Lanzini, A., Brandon, N., Shah, N., 2011. Optimal integration strategies for a syngas fuelled SOFC and gas turbine hybrid. J. Power Sources 196, 9516–9527. https://doi.org/10.1016/j.jpowsour.2011.07.044.